Journal Pre-proof

A multi-proxy study of the Cerro Piche Graben - A Lower Jurassic basin in the central North Patagonian Massif, Argentina

Juan I. Falco, Natalia Hauser, Daniela Olivera, Josefina Bodnar, Wolf Uwe Reimold

PII: S0895-9811(21)00134-6

DOI: https://doi.org/10.1016/j.jsames.2021.103287

Reference: SAMES 103287

To appear in: *Journal of South American Earth Sciences*

Received Date: 28 October 2020

Revised Date: 9 March 2021

Accepted Date: 19 March 2021

Please cite this article as: Falco, J.I., Hauser, N., Olivera, D., Bodnar, J., Reimold, W.U., A multi-proxy study of the Cerro Piche Graben - A Lower Jurassic basin in the central North Patagonian Massif, Argentina, *Journal of South American Earth Sciences* (2021), doi: https://doi.org/10.1016/j.jsames.2021.103287.

Juan I. Falco: Writing, Conceptualization, Resources, Investigation, Review, Funding

Natalia Hauser: Writing, Conceptualization, Resources, Investigation, Review, Funding

Daniela Olivera: Palynology, Writing, Conceptualization, Investigation, Review.

Josefina Bodnar: Paleontology, Writing, Conceptualization, Investigation Review.

Wolff U. Reimold: Writing, Conceptualization, Resources, Investigation, Review, Funding

A multi-proxy study of the Cerro Piche Graben - a Lower Jurassic basin in the central North Patagonian Massif, Argentina.

Juan I. Falco[1,*], Natalia Hauser[2], Daniela Olivera[3,4], Josefina Bodnar[5], Wolf Uwe Reimold[2]

[1]Instituto de Investigaciones en Diversidad Cultural y Procesos de Cambio (IIDyPCa), CONICET - Universidad Nacional de Río Negro, Mitre 630, CP 8400, San Carlos de Bariloche, Argentina.

[2]Laboratorio de Geocronología e Geoquímica Isotópica, Instituto de Geociências, Universidade de Brasília (UnB). Brasília - DF 70910-900, Brazil

[3]Instituto Geológico del Sur (INGEOSUR), Universidad Nacional del Sur-Consejo Nacional de Investigaciones Científicas y Técnicas (CONICET), Av. Alem 1253, cuerpo B´1º Piso, B8000ICN Bahía Blanca, Buenos Aires, Argentina

[4]Departamento de Geología, Universidad Nacional del Sur (UNS), Av. Alem 1253, cuerpo B´ 2do Piso, B8000ICN Bahía Blanca, Buenos Aires, Argentina

[5]División Paleobotánica, Facultad de Ciencias Naturales y Museo, Universidad Nacional de La Plata. Paseo del Bosque s/n, B1900FWA La Plata, Buenos Aires, Argentina

*Corresponding author: falco.juan@gmail.com

Abstract

The volcano-sedimentary succession of the Cerro Piche Graben, Río Negro province, Patagonia (Argentina), was studied U-Pb and Lu-Hf in zircon. As well, a stratigraphic, sedimentological, palynology and a review of the paleo flora content was made. The combined stratigraphic and geochronological study on the volcano-sedimentary succession indicates that the Cerro Piche Graben was developed during the Early Jurassic and allow us to propose the Cerro Piche Formation. This formation is composed of a lower volcanic succession (named the Loma Blanca Member) that is restricted to the tectonic depression and that was probably emplaced during the Sinemurian (ca. 191 Ma), and an upper sedimentary succession (named the El Tono Member) that was unconformably deposited over the lower sequence during the Pliensbachian (ca. 183 Ma). The sedimentological study of the upper sequence allows to recognition of nine sedimentary cycles related to the evolution of an alluvial fan. The palynofacies interpretations reflect intermittent exposure to weathering and/or intense reworking of organic components as a result of a dynamic sedimentary system with a high terrestrial input, sediment reworking, and/or intermittent subaerial exposure. The paleoflora preserved in this sedimentary succession is composed exclusively of conifers and assigned to *Cupessinoxylon* sp., and probably corresponds to an arboreal paleocommunity. The U-Pb data on Early Jurassic detrital zircon grains from the El Tono Member indicate a maximum depositional age (MDA) of 185 Ma for this sequence, and the Lu-Hf data support a reworked continental crust for the zircon source. . Additionally, the U-Pb and Lu-Hf data obtained during this work together with data from the North Patagonian Massif supports the recognition of four magmatic cycles, called C0, C1 (including $C1_i$ source), C2 and C3. The C1 (172-180 Ma)

and the C3 (155-162 Ma) cycles indicate mixing of juvenile mantle-derived and reworked crustal components in the parental magma of zircons and the C0 (182-192 Ma) cycle, which includes the distal volcanism identified in the Cerro Piche Graben, the $C1_i$ (172-180 Ma) and C2 (166-169 Ma) cycles seemingly represent three episodes of crustal reworking.

Keywords: Jurassic volcanism, Patagonia, U-Pb/Lu-Hf isotopes on zircon, Jurassic flora, Stratigraphy.

1. Introduction

Widespread Jurassic volcanism took place in Patagonia during four main episodes. From the Río Negro Province until Tierra del Fuego Province these four volcanic episodes were identified as V0, V1, V2 and V3, which are integrated into the Chon Aike Province (Pankhurst et al., 2000; Franchi et al., 2001; Hauser et al., 2017, Pavon Pivetta et al., 2019). The V0-V1 episodes were related to the Sinemurian and Pliensbachian-Toarcian, respectively (Pankhurst et al., 2000; Pavon Pivetta et al., 2019). These episodes are characterized by the emplacement of within-plate related acidic lavas, ignimbrites and sedimentary rocks of the Marifil Formation, also termed Marifil Complex or Marifil Volcanic Complex (Malvicini and Llambías, 1974; Cortés, 1981; Franchi et al., 2001), which outcrops in northeastern Patagonia on the Atlantic coast (Pankhurst et al., 2020). The V0-V1 volcanic cycles are also contemporaneous with arc activity in the Subcordilleran Patagonian Batholith that lasted until 180 Ma (Rapela et al., 2005), as well as with the early stages of the Andean magmatic arc in the Neuquén Basin (Rosell et al., 2020 and references therein). The second volcanic episode, V2 (Middle Jurassic, 176-162 Ma), occurred in the

eastern part of the Deseado Massif in southern Patagonia. This episode has been related to the high-grade rhyolitic ignimbrites of the Bahía Laura Volcanic Complex, the geochemical characteristics of which suggest a source related to evolved magmas derived from continental crust (Pankhurst et al., 2000). Finally, the V3 episode (Late Jurassic, 157-153) was related to the pyroclastic rocks and associated granites of the eastern Andes (El Quemado Complex – Argentina; and Ibanez Formation – Chile). This last magmatic episode is represented by rhyolitic volcanic rocks outcropping in the Andean region, indicating a western migration of the magmatism and a link with an active margin (Pankhurst et al., 2020).

More recently, Hauser et al. (2017) defined the Cañadón Asfalto magmatic event, which was divided into three magmatic cycles (C1-C3) based on U-Pb and Lu-Hf isotopes in zircons of the Cañadón Asfalto Basin. The C1, called Lonco Trapial Cycle, was developed at ca. 176 Ma and has negative and positive $\varepsilon_{Hf(T)}$ values between -2.2 and +4. The C2, named Las Chacritas Cycle, dated on ca. 168 Ma has negative $\varepsilon_{Hf(T)}$ values, and represents a volcanism that resulted from the reworking of a Mesoproterozoic crust. The C3, named Puesto Almada Cycle and developed at ca. 159 Ma, shows mixed Hf isotope characteristics with $\varepsilon_{Hf(T)}$ values between -5.6 and +2.1 and interpreted as a juvenile magma highly contaminated with old crust. Regarding the V1-V3 episodes (after Pankhurst et al., 2000), Hauser et al. (2017) recognized that these episodes overlap partially with the Cañadón Asfalto magmatic event. The C1 magmatic cycle is bracketed by the V1 and V2 phases, the C2 overlaps exactly with the V2 episode, and the C3 volcanic cycle partially overlaps with the V3 phase.

The Early Jurassic magmatism in northern Patagonia was divided into two domains: the Andean and Extra-Andean (Benedini et al., 2014). The Andean domain includes the Subcordilleran Patagonian Batholith, which corresponds to a belt of subduction related igneous rocks that extends for more than 250 km, representing an oblique batholith developed during Late Triassic–Early Jurassic times (Haller et al., 1999; Rapela et al., 2005; Echaurren et al., 2017; Zaffarana et al., 2020). The extra-Andean domain includes the outcrops of Jurassic volcanic rocks in the NPM. This domain includes the Marifil Volcanic Complex in the eastern part of the NPM; and the Taquetrén (Nullo and Proserpio, 1975), Sañicó (Stipanicic et al., 1968), Garamilla (Nullo, 1978) and Lonco Trapial formations (Lesta and Ferello, 1972), the Comallo Complex (Barros et al., 2020), and the Cañadón Chileno Complex (Benedini et al., 2020) of the central and western part of the NPM. This widespread Jurassic magmatism has been linked with the Karoo mantle plume impingement, related to Gondwana break-up, the opening of the Atlantic Ocean, and westward drifting of Patagonia (Cox, 1992; Pankhurst and Rapela, 1995; Encarnación et al., 1996; Pankhurst et al., 2000; Riley and Knight, 2001; Storey et al., 2013).

In the central part of the North Patagonian Massif, 20 km north of the town of Los Menucos, a relatively small depocenter named the Cerro Piche Graben (CPG – Corbella, 1973) was recently proposed to represent a new Jurassic unit based on the interpretation of fossil trunks and stratigraphic relationships (Falco et al., 2017; Bodnar and Falco, 2018). The aim of the present study is to establish the maximum depositional age and tectonic history of the CPG volcanic/sedimentary rocks, using U-Pb and Lu-Hf isotope analysis on detrital zircon. On the basis of the description of sedimentary facies and palynofacies analysis of selected outcrop samples, a new sedimentological interpretation is

109 presented. All data together will improve the knowledge on the evolution history of the
110 North Patagonian Massif during Mesozoic times with emphasis in the Jurassic.

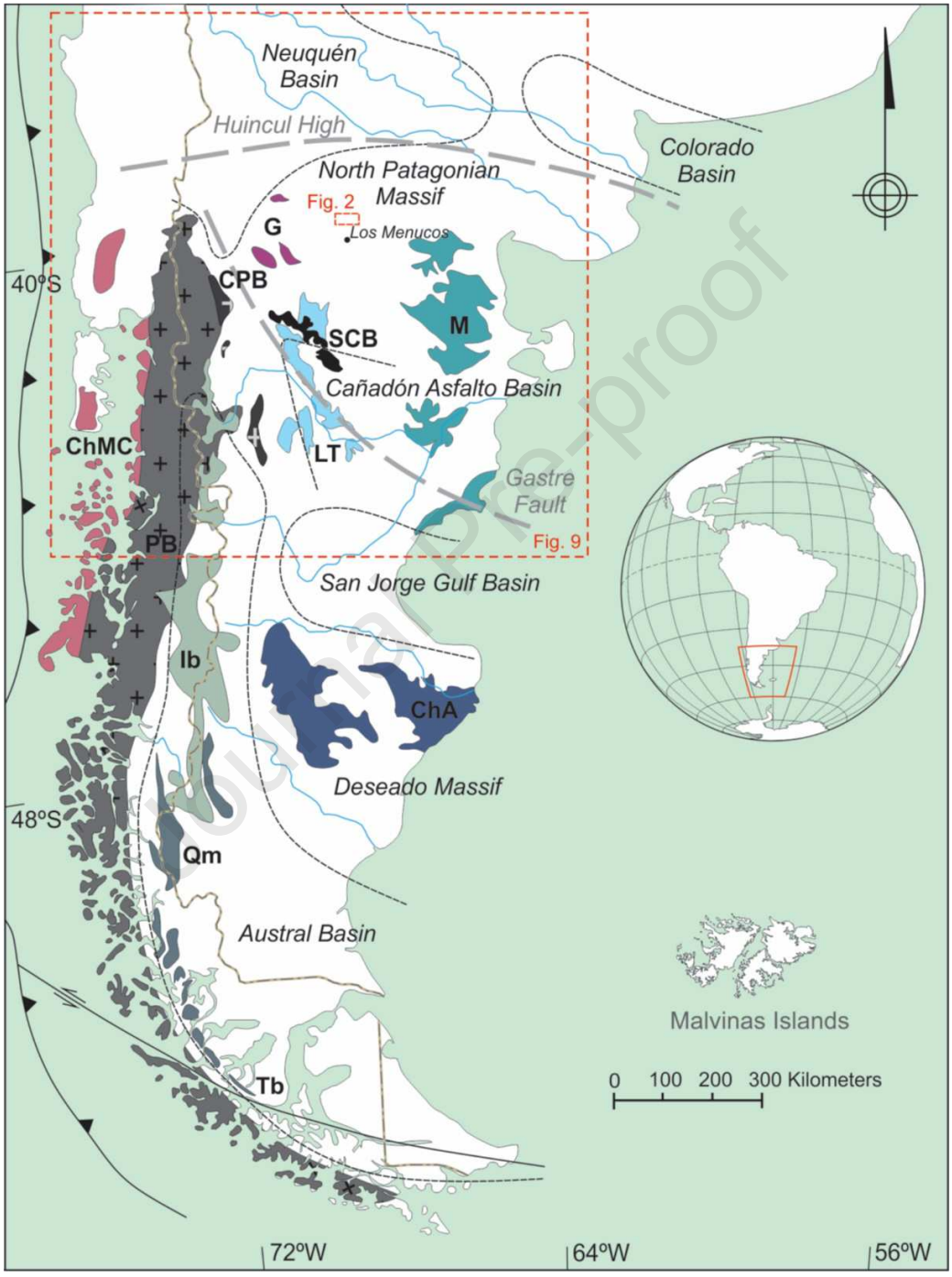

111

Figure 1. Simplified geological map (after Echaurren et al., 2017; Hauser et al., 2017; Pankhurst et al., 2000) showing the main occurrences of Jurassic magmatism in the Patagonian region. The five main Mesozoic basins of southern South America are also depicted: Neuquén Basin, Colorado Basin, Cañadón Asfalto Basin, San Jorge Gulf Basin, and Austral Basin. The positions of the main Huincul and Gastre lineaments are also indicated. G: Garamilla Formation, M: Marifil Formation, CPB: Central Patagonian Batholith, SCB: Subcordilleran Patagonian Batholith, ChMC: Chonos Metamorphic Complex (Late Triassic), PB: Patagonian Batholith (Jurassic–Eocene), LT: Lonco Trapial Formation, Ib: Puesto Ibañez Formation, ChA: Chon Aike Formation, Qm: El Quemado Complex, Tb: Tobífera Formation. See text for a detailed explanation.

2. Geological setting

The NPM (Fig. 1) is a crustal block of approximately 150,000 km^2 between 39 °S and 44 °S in Patagonia of Argentina. This massif is bounded by the Neuquén Basin to the northwest (Upper Triassic–Neogene) and the Colorado Basin to the northeast (Upper Triassic–Neogene). To the south, the NPM is delimited by the Patagonian Precordillera that uplifts Upper Triassic–Lower Jurassic rocks, and the Jurassic Cañadón Asfalto Basin (see Ramos, 1999; Hauser et al., 2017, and references therein). The Paleozoic and Mesozoic stratigraphy of the NPM consists of Cambrian plutonic and metasedimentary rocks, and Ordovician S- and I-type granitoids; all of these are covered by a Silurian to Devonian sedimentary succession in the eastern parts of the NPM (e.g., Ramos, 1999; Pankhurst et al., 2006). Voluminous lower Permian–Middle Triassic magmatism is in evidence along an

E-W belt from the Andes foothills to the Atlantic Coast (Pankhurst et al., 2006; Castillo et al., 2017; Martínez Dopico et al., 2017, 2019, and references therein).

The Jurassic period in the NPM is characterized by extensive volcanic rocks, which also have minor sedimentary interbeds. On the eastern side of the NPM, the Marifil Volcanic Complex has been divided into three formations that unconformably cover the Nahuel Niyeu Formation. The basal Puesto Piris Formation (Nuñez et al., 1975) is composed of red conglomerates, sandstones, black siltstones, limestones, and reworked tuff, with thicknesses between 150 and 550 m. A lava flow assigned to the Marifil Volcanic Complex interbedded in the sedimentary succession of the Puesto Piris Formation was dated to 193 ± 3 Ma (U-Pb in zircon age - Strazzere et al., 2018). The upper units of the Marifil Complex are the Aguada del Bagual (subvolcanic lavas) and La Porfía (agglomerates, tuffs, sandstones and ignimbrites) formations (Cortés, 1981; Márquez et al., 2012). Further south, in the Arroyo Verde area (Río Negro Province), coulées, megabreccias, and lapilli tuffs of the Marifil Formation were assigned to the Sinemurian (U-Pb in zircon age of 193 ± 2 Ma – Pavon Piveta et al., 2019). This Sinemurian volcanic succession is unconformably covered by welded lava-like ignimbrites, massive lapilli tuffs, and rhyolitic lava flows assigned to the Pliensbachian (Pavon Pivetta et al., 2019). Geochemistry suggested that the Sinemurian Marifil Volcanic Complex was generated by partial melting of lower crust related to a dehydrated subducting plate in a back-arc setting, whereas the Pliensbachian magmatism originated from partial melting of the mafic lower crust, induced by a mantle plume impingement (Pankhurst and Rapela, 1995; Pankhurst et al., 2000; Pavon Pivetta et al., 2019).

In the western NPM, the Taquetrén (Nullo and Proserpio, 1975) and Garamilla (Nullo, 1978) formations and the Comallo (Barros et al., 2020) and Cañadón Chileno (Benedini et al., 2020) complexes are well exposed from the Limay river to the Sierra de Taquetrén locality (all indicated as G in Fig. 1). The Taquetrén Formation consists of breccias, lavas, tuffs and ignimbrites of andesitic composition, and is interpreted as volcaniclastic facies of the Lonco Trapial Formation, which belongs to the Cañadón Asfalto Basin (Lesta and Ferello, 1972, Lizuaín and Silva Nieto, 2005). The Pliensbachian Garamilla Formation (U-Pb zircon age of 189 ± 1 Ma – Benedini et al., 2014) is characterized by ignimbrites, breccias, tuffs, and lavas of mainly intermediate to rhyolitic composition, revealing a progressive change from a subduction to an intraplate-related tectonic setting (Benedini et al., 2014). The Comallo Complex has been related to a NW-SE pull-apart volcanic depocenter of Sinemurian age (U-Pb zircon age of 192 ± 3 Ma, Barros et al., 2020). Volcanic products, including pyroclastic and coherent volcanic rocks, as well as a few sedimentary deposits, characterize the lower section of the Comallo Complex. The upper section is dominated by red beds deposited in a fluvial sedimentary environment (Barros et al., 2020). The Cañadón Chileno Complex (Benedini et al., 2020) is a small asymmetrical volcanic and sedimentary depocenter, which has been dated to the Pliensbachian (U-Pb zircon age of 188 ± 3 Ma – Benedini et al., 2020).

To the south of the NPM, the volcano-sedimentary sequence of the Cañadón Asfalto Basin (Fig. 1) was also developed during the Jurassic. It is considered a sinistral pull-apart basin that was developed according to older lineaments such as the Gastre system (Silva Nieto et al., 2002). Although the stratigraphy of this basin is still discussed (e.g., Cúneo et al., 2013; Hauser et al., 2017), U-Pb zircon geochronology supports that this basin

179 evolved from the Pliensbachian (Early Jurassic) until the Kimmeridgian (Late Jurassic)
180 (Cúneo et al., 2013; Bouhier et al., 2017; Hauser et al., 2017).

181 Cretaceous and Paleogene–Neogene sedimentary rocks, and the upper
182 Oligocene to lower Miocene Somuncurá Basaltic Plateau cover all these Jurassic units of
183 the NPM (Ramos, 1999; Asiain et al., 2019).

184

185 ***2.3. Local geological setting***

186 The Cerro Piche Graben (CPG - Corbella, 1973) is a 40 km long, E-W
187 trending gravitational structure located 30 km north of Los Menucos town in the central
188 North Patagonian Massif (Figs. 1, 2). The best exposures of the CPG are delimited to its
189 eastern sector of the graben by the Queupuniyeo Range, and to the west by the Bajos
190 Hondos Basaltic Plateau (Fig. 2). This tectonic structure, also mentioned as Piche Fault
191 System or pull-apart Piche (Giacosa et al., 2007), is part of a major family of E-W faults
192 recognized in the surrounding area, such as the Loma Blanca fault (Cucchi et al., 2001), as
193 well as the La Laja and La Laja Norte faults (Giacosa et al., 2007), inter alia.

194 The CPG is limited by two subparallel faults (Fig. 2). The northern fault cuts
195 across granitic and volcanic rocks of the La Esperanza Complex (see Martínez Dopico et
196 al., 2017, 2019) and the low-grade metamorphic rocks of the Colo Niyeu Formation
197 (Labudia and Bjerg, 1994). The southern fault also cuts the Colo Niyeu Formation and the
198 La Esperanza Complex, as well as the eastern sector of the Los Menucos Group or
199 Complex (Lema et al., 2008; Falco et al., 2020).

The Colo Niyeu Formation is a 1500 m succession of metasedimentary rocks, mainly characterized by quartzitic and phyllitic beds, which were affected by low-grade metamorphism (Labudia and Bjerg, 1994). The age of this metamorphic succession is still debated between Cambrian (Martínez Dopico et al., 2017) or younger than Devonian (Chernicoff et al., 2018). The La Esperanza Complex has been dated between ca. 273 and 244 Ma, and a series of granitic and granodioritic plutons, mesosilicic lavas, ignimbritic layers, and rhyiolitic dikes have been grouped together in this complex (see Martínez Dopico et al., 2019 and references therein).

The Los Menucos Group or Complex and its stratigraphy are still under debate (see Falco et al., 2020 and references therein). Initially, the volcanic and sedimentary succession of the CPG was considered the lowermost part of the Los Menucos Group (Labudia and Bjerg, 2001) or Los Menucos Complex (Giacosa et al., 2007). Recently, Falco et al. (2020) reviewed the stratigraphy and proposed a subdivision for the Los Menucos Group (after Labudia and Bjerg, 2001) into a series of ignimbrites, mesosilicic lavas and sedimentary layers that were emplaced during the interval of 253 to 248 Ma. In this new stratigraphic proposal, the CPG succession was considered as a younger episode than the Los Menucos Group, possibly emplaced during the Jurassic (see Bodnar and Falco, 2018; Falco et al., 2020). Similarly, Cucchi et al. (2001) named andesitic lavas of this succession as the Vulcanitas Loma Blanca (Loma Blanca volcanic rocks). Some of these lavas were emplaced along the E-W faults of the graben and also tentatively assigned to the Jurassic.

The CPG contains a ~500 m volcano-sedimentary succession (Corbella, 1973; Labudia et al., 1992; Bodnar and Falco, 2018). Labudia et al. (1992) described this

succession as deposited by ephemeral fluvial systems with channels activated during rainy seasons. This sedimentary succession includes fossil trunks described as *Pleuromeia* sp. (Labudia et al., 1992), suggesting an Early to Middle Triassic age for these rocks (Labudía and Bjerg, 2001; Giacosa et al., 2007; Lema et al., 2008). Later, new paleontological studies reassigned the fossil trunks to *Cupressinoxylon* sp., discarding an exclusively Triassic age (Bodnar and Falco, 2018, see also Falco et al., 2020). The age of these deposits is still unclear; the current state of knowledge suggests deposition after the Los Menucos Group, possibly during Jurassic times (Corbella, 1973; Falco et al., 2017; Bodnar and Falco, 2018).

Finally, tectonic and deformational studies of the CPG indicate that dextral E-W faults with kilometer-scale displacement were linked with a NE-SW to NNE-SSW oblique extension, possibly following older lineaments (Giacosa et al., 2007). These E-W structures also show earlier reactivation during the Miocene, which facilitated the extrusion of basalts, such as the Cerro Piche and other minor monogenetic bodies (Corbella, 1973; Giacosa et al., 2007).

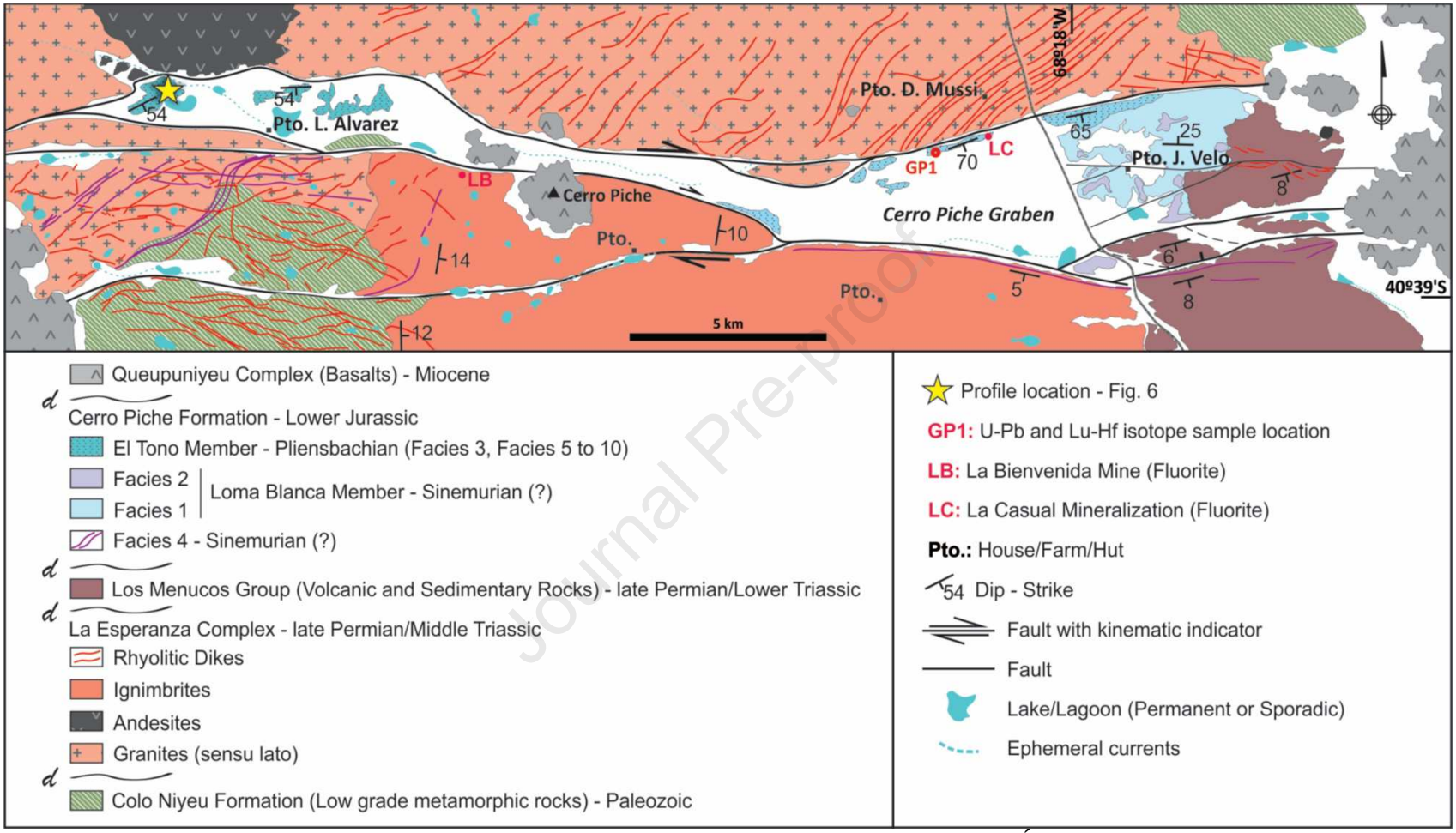

Figure 2. Detailed geological map of the study area; the yellow star to the northwest of Pto. L. Álvarez indicates the measured profile presented in Fig. 6. Structural configuration after Giacosa et al. (2007).

3. Material and methods

Fieldwork involved standard profiling techniques, description of igneous and sedimentary facies, and their stratigraphic relationships. At Puesto L. Álvarez, where the sedimentary succession is best exposed (Fig. 2, 6), a complete sedimentary profile was measured. At the same profile, fine-grained Facies 5 (see below) was sampled for palynological studies (Fig. 5, 6). The sample of Facies 10 for U-Pb and Lu-Hf isotope in zircon analysis was collected to the south of Puesto D. Mussi (Fig. 2, 4, 7).

3.1. U-Pb and Lu-Hf isotopes on zircon

For the U-Pb and Lu-Hf isotope study on zircon, a 5 kg rock sample was crushed and then sieved to different size fractions (100 to 400 μm) in the Laboratorio de Petrotomía de la Universidad Nacional del Sur (Bahía Blanca, Argentina). After handpicking, the zircon grains were cast into an epoxy mount, polished to approximately half thickness, and the polished surfaces were characterized by back-scattered electron (BSE) and cathodoluminescence (CL) imaging using a FEI QUANTA 450 scanning electron microscope (SEM) at the Laboratory of Geochronology and Isotope Geochemistry of the Universidade de Brasília. These images provided the basis for selecting potential locations in the grains for laser-ablation analysis. U-Pb and Lu-Hf isotope analyses were performed using a Thermo-Fisher Neptune HR-MC-ICP-MS coupled with a Nd:YAG UP213 New Wave laser ablation system.

U-Pb analyses (see data Table in the Supplementary Material) were performed based on the standard-sample bracketing method (Albarède et al., 2004) using the GJ-1 standard (Jackson et al., 2004) in order to monitor ICP-MS fractionation. The 91500 reference zircon (Wiedenbeck et al., 1995, 2004) was also analyzed as a secondary reference material during the analytical sessions. Tuned masses were 238, 207, 206, 204 and 202. Integration time was 1 second and ablation time was 40 seconds. Spot size was 25 µm and laser adjustment was 10 Hz and 2-3 J/cm^2. In addition, the $^{207}Pb/^{206}Pb$ and $^{206}Pb/^{238}U$ ratios were time corrected.

Common ^{204}Pb was monitored based on the ^{202}Hg and ($^{204}Hg+^{204}Pb$) masses. Common Pb corrections were not carried out during this investigation due to very low signals for ^{204}Pb (<30 cps) and high signals for the $^{206}Pb/^{204}Pb$ ratios. Reported errors were propagated by the quadratic addition [(2SD ^ 2 + 2SE ^ 2) 1/2] (SD = standard deviation; SE = standard error) of external reproducibility and performance accuracy. External reproducibility was represented by the standard deviation based on repeated analyses (n= 20, ~1.1% for $^{207}Pb/^{206}Pb$ and up to ~2% for $^{206}Pb/^{238}U$) of the GJ-1 zircon standard during the analytical sessions, whereas performance accuracy was the standard error calculated for each analysis. Weighted mean ages were calculated with the Isoplot-3/Ex software (Ludwig, 2012). The adopted geological time scale follows the one used by Cohen et al. (2013, updated).

Lu-Hf isotopes were analyzed on zircon grains that had been previously analyzed for U-Pb isotopes and that had given concordant data (ratio between $^{206}Pb/^{238}Pb$ and $^{207}Pb/^{235}U$ apparent ages). Whenever possible, both the U-Pb and Lu-Hf analysis points were set as close as possible to enable an analysis of zircon grain portions with the same

isotopic ages. Before the Hf isotope measurements, replicate analyses of a 200 ppb Hf JMC 475 standard solution doped with Yb (Yb/Hf = 0.02) were carried out ($^{176}Hf/^{177}Hf$ = 0.282162±13 2s, n= 4). The analysis of the GJ-1 standard was replicated during the analytical session and recorded a $^{176}Hf/^{177}Hf$ ratio of 0.282006 ± 16 (2σ, n= 25), as compared to the reference value of 0.282000 ± 0.000005 by Morel et al. (2008) for this standard. The value recorded for GJ-1 was 0.282015 ± 0.000009 (n= 5.2 SD) at an intensity of 2.03 ± 0.08 V for ^{178}Hf. The Lu-Hf isotope data were collected for 40-50 seconds of ablation, yielding 40 μm spot diameters, and for 85% energy. The signals of the interference-free isotopes ^{171}Yb, ^{173}Yb and ^{175}Lu were monitored during analysis in order to correct for isobaric interferences of ^{176}Yb and ^{176}Lu on the ^{176}Hf signal. The ^{176}Yb and ^{176}Lu contributions were calculated using the isotopic abundance of Lu and Hf proposed by Chu et al. (2002). Contemporaneous measurements of ^{171}Yb and ^{173}Yb provide a means to correct for mass-bias of Yb using a $^{173}Yb/^{171}Yb$ normalization factor of 1.132685 (Chu et al., 2002). Hafnium isotope ratios were normalized to the $^{179}Hf/^{177}Hf$ value of 0.7325 (Patchett, 1983). A detailed description of procedures and methods was provided by Matteini et al. (2010).

The $\varepsilon_{Hf(T)}$ values of each grain were recalculated for the U-Pb age that had been previously recorded for the same zircon grain. The $\varepsilon_{Hf(T)}$ values were calculated based on the decay constant $\lambda = 1.86*10^{-11}$ suggested by Scherer et al. (2006), as well as on the $^{176}Hf/^{177}Hf$ and $^{176}Lu/^{177}Hf$ CHUR values (0.282786 and 0.0336, respectively) suggested by Bouvier et al. (2008). Depleted mantle Hf model ages (T_{DM} Hf) were calculated based on the $^{176}Hf/^{177}Hf$ and $^{176}Lu/^{177}Hf$ DM values (0.28325 and 0.0384, respectively) suggested by Chauvel and Blichert-Toft (2001). The value of $^{176}Lu/^{177}Hf$ ratio (0.0113) was used as

mean crust reference (Taylor and McLennan, 1985; Wedepohl, 1995). Thus, T_{DM} ages were calculated based on the initial Hf isotopic composition of zircon by using mean Lu/Hf crustal values (Gerdes and Zeh, 2009; Nebel et al., 2007). The initial Hf composition of zircon represented the $^{176}Hf/^{177}Hf$ value, which was calculated at the zircon crystallization time, based on the U-Pb age previously recorded for the same crystal.

3.2. Palynofacies analysis: laboratory treatments and microscopy techniques

Three palynological samples were studied (Fig. 5, 6). The physical and chemical extraction of the palynological matter (PM) was carried out at the Laboratorio de Palinología of the Instituto Geológico del Sur (INGEOSUR)/Universidad Nacional del Sur (UNS)-Bahía Blanca. All samples were prepared according to standard non-oxidative palynological techniques, which involved treatments with hydrochloric and hydrofluoric acids. This residue was used to prepare a first palynofacies slide, in which a general visual assessment of the complete palynological assemblage was done. Then, the remaining residues were sieved using a 10-µm mesh according to Tyson (1995) and a second slide was prepared. The slides were examined using a transmitted white-light microscope (Olympus BX40) and a reflected fluorescent light microscope (RFL; Olympus BH2) with the goal of assessing the preservation state of the PM. The description of the organic particles is based on terminology adapted from Batten (1983, 1996), Tyson (1995), and Oboh-Ikuenobe and de Villiers (2003). At least 500 particles were point-counted per slide using a 40x objective for the second slide. The Palynofacies Types (i.e., the different associations of PM) are defined based on this account. The term Palynofacies Type describes a specific palynological matter assemblage thought to reflect particular

environmental conditions (Brugman et al., 1994, and references therein). The organic content of the sediments behaves in the same way as clastic particles (e.g., Traverse, 1994; Tyson, 1995). Thus, the results of the palynological study correlated with the outcomes of a sedimentary analysis constitute a useful tool for reconstructing sedimentary processes. The palynological slides are housed in the INGEOSUR/UNS; they are identified by a catalogue number preceded by the abbreviations UNSP (Universidad Nacional del Sur, Palinología).

4. Results

4.1. Facies description

In the course of fieldwork in the CPG, 10 facies (Table 1; Fig. 3, 4, and 6) were recognized.

4.1.1. Facies 1: Columnar jointed andesite

This facies is restricted to the graben (Fig. 2) and crops out in the environs of Puesto J. Velo. This andesite is characterized by porphyritic to glomeroporphyritic texture where aggregates of plagioclase, biotite, and hornblende phenocrysts are inserted in an intersertal groundmass composed of plagioclase microliths and glass. The plagioclase phenocrysts can be divided into two groups: the first one of larger and zoned crystals of euhedral shape (~3 mm), and the second one with smaller crystals (~400 µm) without zonation and anhedral shape. Meta-sandstone and granitoid fragments are common inclusions in this facies, which are tentatively related to the Colo Niyeu Formation and the La Esperanza Complex (Permian). This facies represents cooling of a lava flow, which was exclusively emplaced into the tectonic depression.

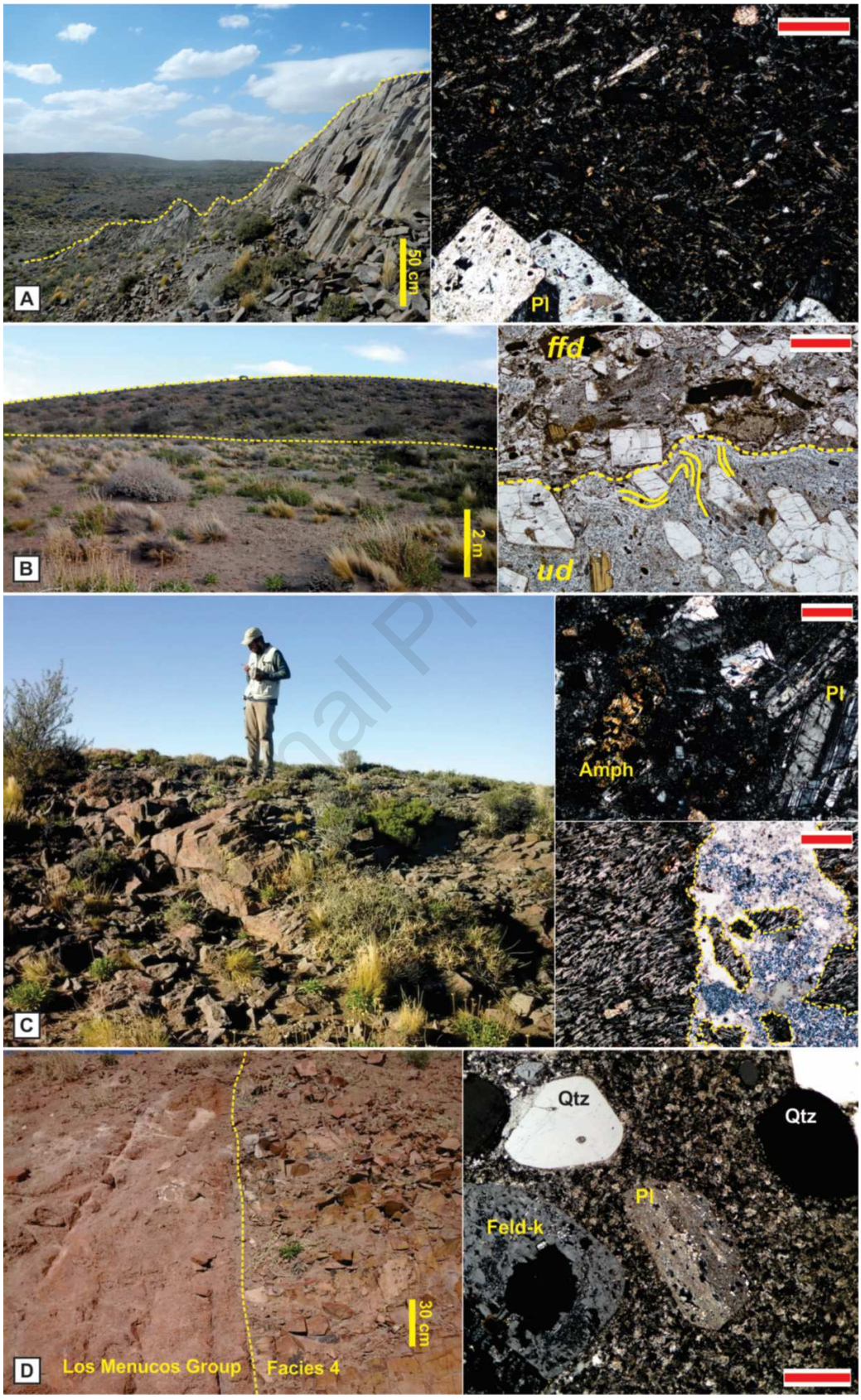
A
50 cm
Pl
B
2 m
ffd
ud
C
Pl
Amph
D
Los Menucos Group
Facies 4
30 cm
Qtz
Qtz
Pl
Feld-k

354

Figure 3. Facies 1 to 4 outcrop photographs. Yellow dotted lines indicate the skyline or boundaries in outcrop; the photos on the right side (insets) show microscopic textural features for each facies. (A) Facies 1, columnar jointed andesite. (B) Facies 2, flow foliated rhyolite lava. Figure inset, the flow-foliated domain (ffd) and the undisturbed domain (ud). The yellow lines on the undisturbed domain highlight the foliated groundmass around phenocrysts. (C) Facies 3, massive andesite. Upper inset shows the textural arrangement of the facies, the lower inset shows the secondary brecciated texture infilled (yellow dotted lines) with quartz, fluorite and calcite. (D) Facies 4, massive rhyolite dikes cutting across ignimbritic deposits of the Los Menucos Group at the southern end of the graben. (A), (B) and (C) from the Puesto J. Velo area and (D) from the Puesto D. Mussi area. The red scale bar in the microscope photography of each facies represents 500 µm. Pl: plagioclase, Amph: amphibol, Qtz: quartz, Feld-K: potassium feldspar. Abbreviations based on Siivola and Schmid (2007)

4.1.2. Facies 2: Flow-foliated rhyolite

Like Facies 1, the flow-foliated porphyritic rhyolitoid lava of Facies 2 is restricted to the eastern part of the graben. Phenocrysts are euhedral plagioclase, quartz, biotite, and hornblende (Fig. 3B) that are immersed into a fresh vitric groundmass. The flow foliation is recognizable as two different domains that are both monocompositional (Fig. 3B). One domain shows massive undisturbed texture with euhedral crystals and vitric groundmass; and the second, flow-foliated domain exhibits brecciated texture, with foliated vitric groundmass around phenocrysts (Fig. 3B). This facies represents the cooling of a rhyolite lava flow.

Facies	Description	Interpretation
Facies 1: Columnar jointed andesite	Texture: porphyritic to glomeroporphyritic Phenocrysts: plagioclase, biotite, hornblende Groundmass: intersertal with plagioclase microliths	Cooling from a lava flow
Facies 2: Flow foliated rhyolite	Texture: Porphyritic Phenocrysts: plagioclase, quartz, biotite, hornblende Groundmass: vitric	Cooling from a lava flow
Facies 3: Massive andesite	Texture: Porphyritic Phenocrysts: plagioclase, amphibole Groundmass: trachytic – calcite replaced Secondary brecciation infilled with fluorite	Cooling from a lava flow
Facies 4: Massive rhyolite dikes	Texture: porphyritic to glomeroporphyritic Phenocrysts: quartz, K-feldspar, plagioclase Groundmass: totally replaced to K-feldspar	Cooling from an ascending lava flow
Facies 5: Massive tuff	Texture: fragmentary Clasts: *Y*, *X*, and *platy* glass shards, quartz, lithic clasts Fossil content: *Cupressinoxylon* sp., leaves, shells, palynological matter	Ash fall deposit
Facies 6: Clast-supported conglomerate	Internal organization: cross to horizontal, crude stratification Shape: Channelized deposits Clast origin: volcanic, granitic and metamorphic rocks Matrix: sandy	Deposited by high-energy, unidirectional, tractive flows or fluidized debris flows, infilling minor channels or as longitudinal bedforms. Paleocurrents: S, SW, SE
Facies 7: Matrix-supported conglomerate	Internal organization: massive, normal- to inverse-grading. Shape: lobate or convex-up, with non-erosional bases Clasts origin: volcanic, granitic and metamorphic rocks	Deposited by unidirectional flows, with high sediment concentration, and high internal strength. Paleocurrents: S

	Matrix: sandy	
Facies 8: Massive coarse-grained sandstone	Internal organization: massive to faintly laminated. Shape: tabular Clast origin: volcanic, granitic and metamorphic rocks, quartz, k-feldspar, plagioclase and biotite. Matrix: scarce, fine-grained	Deposited by sediment-gravity flows
Facies 9: Medium to fine grained sandstone	Internal organization: cross-stratification (planar, trough and low-angle), cross-lamination with normal grading, horizontal lamination. Shape: channelized, tabular or mantled Clast origin: volcanic, granitic and metamorphic rocks, quartz, k-feldspar, plagioclase. Matrix: scarce, fine-grained	Deposited by tractive flows. Trough and planar cross-stratified sandstones are related to fluvial channels and migration of 2D and 3D dunes, horizontally and low-angle cross-stratified sandstone can be linked to washed out dunes or an upper flow regime. Cross-laminated sandstones are related to ripple migration. Paleocurrents: S, SW, SE, N, E, W.
Facies 10: Massive to fine laminated mudstone and sandstone	Internal organization: interbedded fine-grained sandstone and mudstone; the sandstones occasionally develop small current ripples or symmetrical ripples. Shape: tabular Clast origin: quartz and glass shards, with minor biotite, K-feldspar, and clay minerals. Fossil content: *Cupressinoxylon* sp., leaves	Deposited by settling, with minor influence of tractive flows. Paleocurrents: S, SW, SE, N, E.

Table 1. Summary of the characteristics of the 10 facies recognized in the Cerro Piche Graben.

380 *4.1.3. Facies 3: Massive andesite*

381 The massive andesite is also restricted to the eastern part of the study area
382 and is restricted to the graben. The poorly exposed outcrops are aligned along the E-W
383 faults (Fig. 3C). The texture of the massive andesite is porphyritic with trachytic
384 groundmass, which is partially to totally replaced by calcite. The phenocrysts are anhedral
385 to euhedral plagioclase and amphibole. This massive andesite displays an intense secondary
386 brecciation with fractures infilled with quartz, calcite and fluorite. This secondary overprint
387 is tentatively related to the fluorite mineralization at the La Bienvenida and La Casual
388 mines (Figs. 2 and 3C). This facies represents cooling from a lava flow, and its extrusion
389 was controlled by faulting.

390

391 *4.1.4. Facies 4: Massive rhyolite dikes*

392 This is the only facies recognized outside of the tectonic depression. In the
393 eastern area, these dikes are extended parallel to the E-W structure of the graben. In the
394 western area, to the south of Puesto L. Álvarez, a NE-SW sigmoidal dike swarm intruded
395 into the Colo Niyeu Formation, which is bounded by two parallel E-W trending faults (Fig.
396 2). The dikes have thicknesses up to 3 m, are pink colored, and they have porphyritic to
397 glomeroporphyric textures. Phenocrysts are quartz, K-feldspar, and plagioclase (Fig. 3D),
398 and groundmass is totally recrystallized. Quartz is anhedral, fresh and normally it has
399 embayments. K-feldspar is strongly altered but subhedral shapes are still recognizable;
400 plagioclase crystals are comparatively the smallest and have subhedral to anhedral shape
401 (Fig. 3D). This facies represents cooling from an ascending lava emplaced along E-W or

sigmoidal structures related to the development of the CPG structure (see also Giacosa et al., 2007).

4.1.5. Facies 5: Massive tuff

This facies belongs to the sedimentary succession that fills the graben, and it is mainly recognized in the upper part of the graben fill. It is a light brown, massive tuff exposed as loose debris or blocks (Fig. 4A). Under the microscope, the texture of this rock is fragmentary. It is predominantly composed of glass shards, small crystalloclasts, and lithic clasts. Glass shards show *Y*, *X*, and *platy* shapes and were deposited parallel to depositional planes. The crystalloclasts are mainly composed of quartz, and their shapes are often triangular. Scarce lithic clasts are rounded to sub-rounded and derived from volcanic and sedimentary rocks. This facies bears shell imprints, small pieces of carbonized wood, leaves, and fossil trunks of *Cupressinoxylon* sp. (Bodnar and Falco, 2017). This lithology was sampled for palynological analysis (Samples UNSP4514, UNSP4515 and UNSP4516). This facies was deposited by ash fall, and the recognition of shell imprints is indicative of deposition into water bodies. The rounded lithic clasts recognized in this facies suggest that these deposits were probably related to a local epiclastic input/reworking.

4.1.6. Facies 6: Clast-supported conglomerate

This facies, a reddish-brown to dark brown, clast-supported conglomerate (Fig 4B), mostly occurs at the bottom of the sedimentary succession, with minor occurrences in the middle section, and it is absent towards the top (Fig. 6). . The internal

organization varies from cross to horizontal, crude stratification; the base is erosive resulting from channelized deposits, and the vertical arrangement tends to normal grading. Lateral extension of these deposits can reach tens of meters, and thickness is up to 2.5 m. Clasts are derived from volcanic, granitic, and metamorphic rocks and they are subangular to subrounded. Sandy matrix is composed of quartz and feldspar, of subangular to subrounded shape; occasionally matrix shows a considerable proportion of glass shards. Field relations indicate that this facies is linked with Facies 7, 8 and 9. This facies was deposited by high-energy, unidirectional, tractive flows or fluidized debris flows, infilling minor channels or as longitudinal bedforms. Clast imbrication and primary sedimentary structures indicate that flow direction was predominantly towards the S, with minor variations to SW and SE.

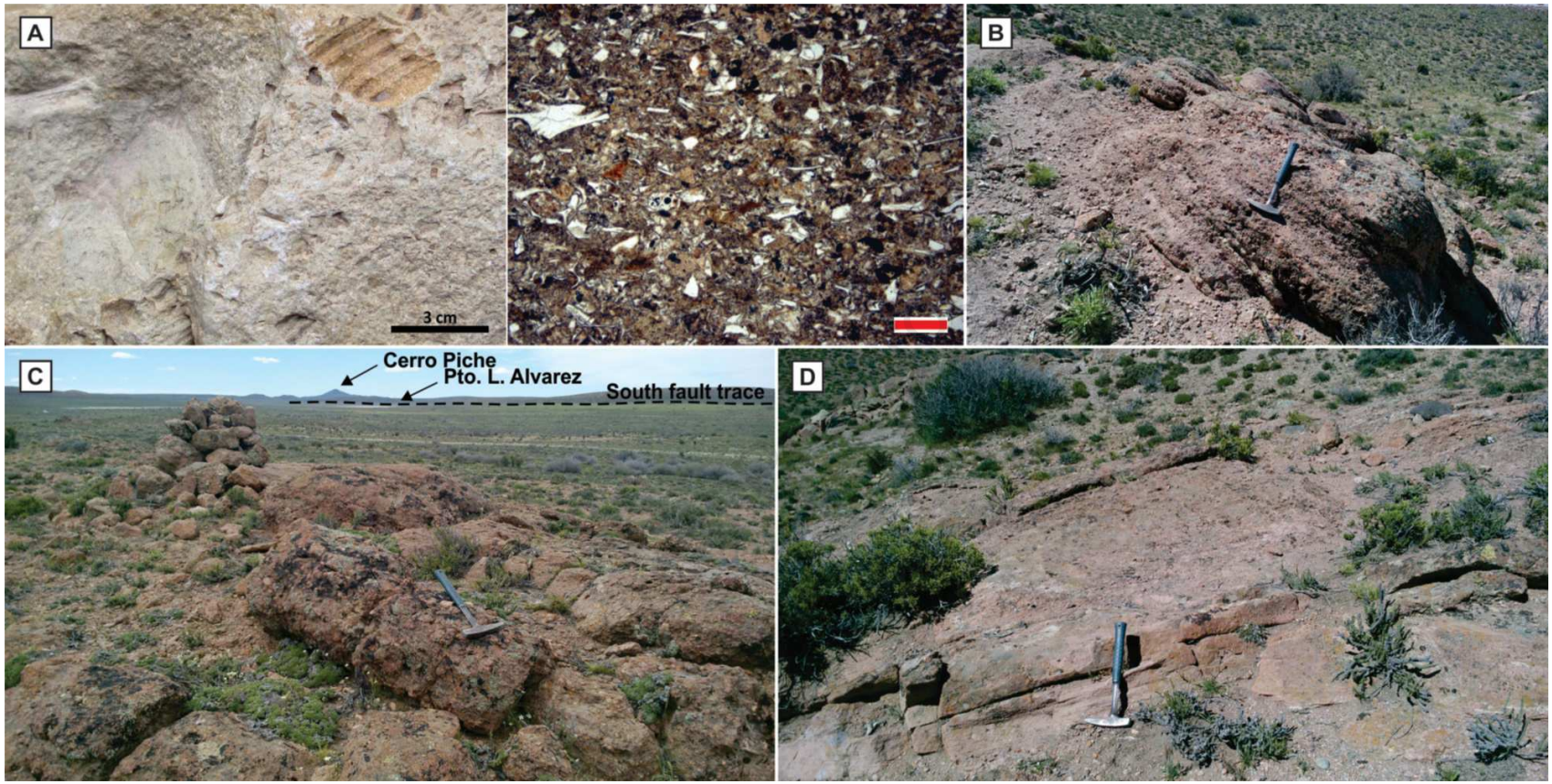

438

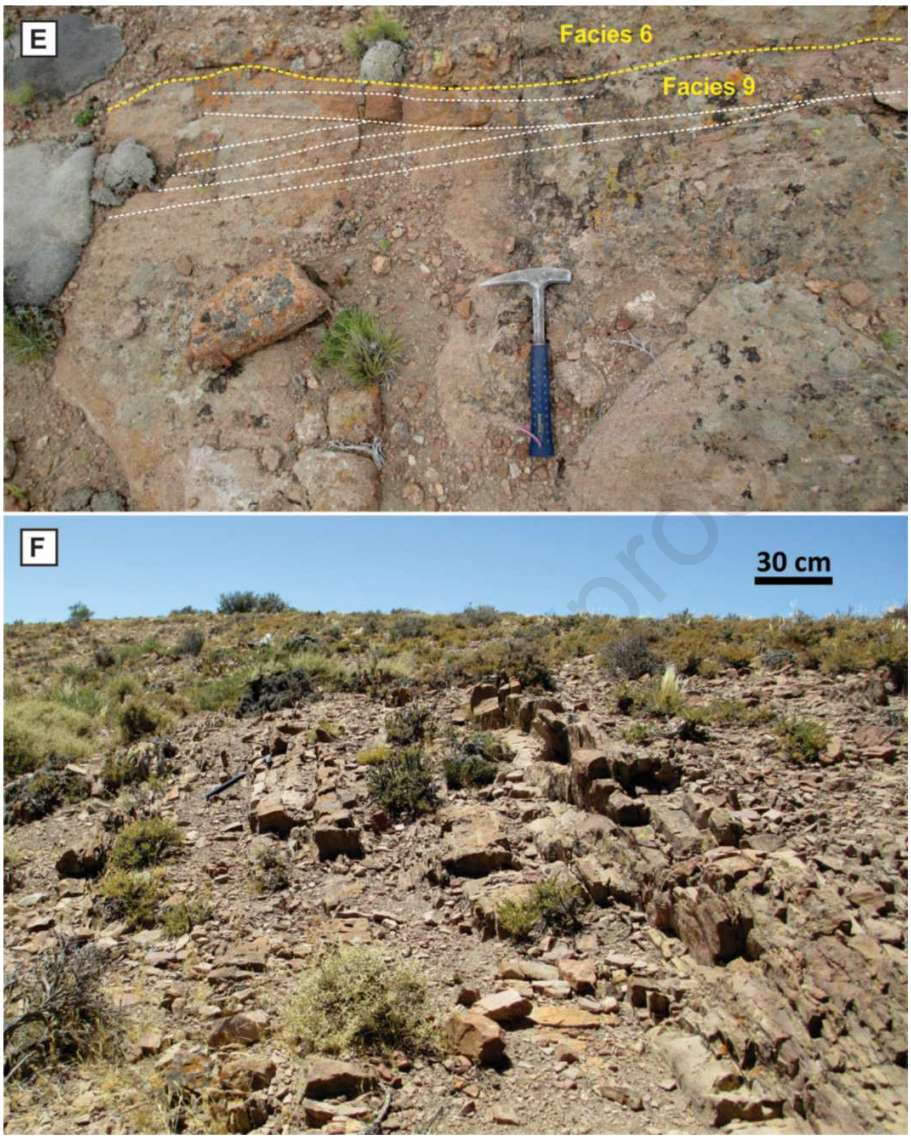

Figure 4. Ouctrop images for Facies 5 to 10. Yellow dotted line indicates facies contact; white dotted lines indicate sedimentary structures. Figures (A) to (E) show the sedimentary succession at Pto L. Álvarez, whereas the photo in (F) was taken at Pto D. Mussi where Facies 10 was sampled for U-Pb and Lu-Hf isotopic analysis on zircon. (A) Facies 5, massive tuff where a shell mold is shown. The microscopic texture is also shown to the right; the red scale bar in the photo on the right is 600 µm in width. (B) Facies 6, clast-supported conglomerate. (C) Facies 7, matrix-supported conglomerate. (D) Facies 8,

447 massive coarse-grained sandstone. (E) Facies 9, medium- to fine-grained sandstone; note
448 the erosive contact between Facies 6 and 9 (yellow dotted line). (F) Facies 10, massive to
449 fine-laminated mudstone and sandstone.

450

451 *4.1.7. Facies 7: Matrix-supported conglomerate*

452 This facies is also restricted to the lower half of the sedimentary succession.
453 Facies 7 is a reddish-brown, matrix-supported, massive conglomerate. The vertical
454 arrangement varies from normal- to inverse-grading (Fig 4C). The shape of matrix-
455 supported conglomerate bodies is mainly lobate or convex-up, with non-erosional bases.
456 Lateral extension could not be determined; thickness is up to 4 m. Clasts are mainly angular
457 to subangular and also derived from volcanic, granitic, and metamorphic rocks. The matrix
458 is sandy and composed of quartz, feldspar, biotite, lithic clasts, and a minor amount of tuff.
459 This facies was deposited by unidirectional flows, with high sediment concentration, and
460 high internal strength. Although paleocurrent directions could not be measured, deposit
461 shapes suggest a mainly south-directed flow direction.

462

463 *4.1.8. Facies 8: Massive coarse-grained sandstone*

464 This facies, a reddish brown to greenish gray, coarse-grained to pebbly
465 sandstone (Fig. 4D), is restricted to the lower half of the sedimentary succession. . Deposits
466 are tabular, and the internal arrangement is mainly massive to faintly laminated (to the top).
467 Lateral extension is on the scale of tens of meters and thickness is up to 2 m. Fabric varies
468 between matrix- and clast-supported, and the clasts vary from angular to subangular in

shape. There are quartz, K-feldspar, plagioclase, and biotite, as well as volcanic, plutonic, and metamorphic lithic clasts. This facies was deposited by sediment-gravity flows.

4.1.9. Facies 9: Medium- to fine-grained sandstone

This facies is recognized in the lower half of the sedimentary succession. It is a light-brown, medium- to fine-grained sandstone with a clast-supported fabric. Internal organization shows cross-stratification (planar, trough and low-angle) to cross-lamination with normal grading; horizontal lamination is also occasionally present. This deposit has a channel shape when it is cross-stratified, or it is tabular or mantled when horizontally or cross-laminated. Lateral extension is highly variable up to tens of meters, and thickness is up to 6 m. Clasts have sub-angular to sub-rounded shape and are quartz, K-feldspar, plagioclase, and lithic clasts from granites, and metamorphic and volcanic rocks. This facies was deposited by tractive flows. Trough and planar cross-stratified sandstones are related to fluvial channels and migration of 2D and 3D dunes, horizontally and low-angle cross-stratified sandstones can be linked to washed out dunes or an upper flow regime. Cross-laminated sandstones are related to ripple migration. Paleocurrent direction measurements reveal considerable variation of transport direction. In the lower part of the succession, the main flow direction is towards the S, with variation to the SE and SW; in contrast, in the upper part of the deposit, the flow direction occasionally also assumes N, E or W directions.

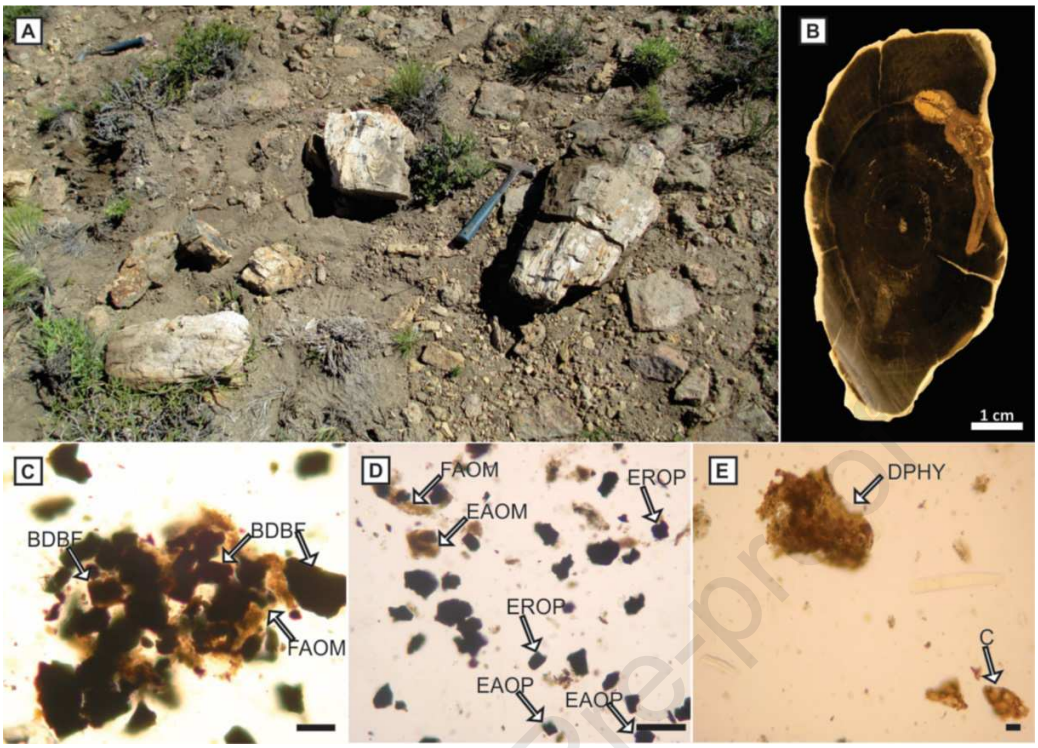

Figure 5. Fossil images. (A) Fragments of the *Cupressinoxylon* sp. trunks from NW of Pto. L. Álvarez. (B) Polished surface of the permineralized axis of *Cupressinoxylon* sp (after Bodnar and Falco, 2018). (C-D) Photomicrographs of the identified palynofacies types (PT). (C) PT-UNSP4514, sample UNSP4514: J32/0; BDBF: black or dark brown fragments, FAOM, fibrous amorphous organic matter. (D) PT- UNS4515, sample UNSP45145: O37/4; EAOP: equidimensional opaque phytoclasts with angular edges, EROP: equidimensional opaque phytoclasts with rounded edges, EAOM: spongy amorphous organic matter. (E) UNS4516 sample: O49/3; DPHY, degraded phytoclasts, C, small pieces of partially degraded cuticles. Black-line scale bar in figures C-E is 10 μm long.

4.1.10. Facies 10: Massive to fine-laminated mudstone and sandstone

This is the most common facies in the upper part of the sedimentary succession. It comprises interbedded fine-grained sandstone and mudstone; the sandstones occasionally develop small current ripples or symmetrical ripples (Fig. 4F). The more common clasts are quartz and glass shards; minerals as biotite, K-feldspar, and clay minerals are also present. Lateral extension could not be determined, but seems to be at the scale of hundreds of meters; thickness is on the scale of tens of meters. These deposits bear leaf impressions and fossil trunks of *Cupressinoxylon* sp. (Corbella, 1973; Bodnar and Falco, 2018) (Fig. 5). One sample (Sample GP1) was taken for U-Pb and Lu-Hf isotopic analysis on zircon on the eastern side of the graben, to the south of Puesto D. Mussi (Fig. 2).

This facies was deposited by settling, with minor influence of tractive flows. The measured paleocurrent directions for sandy beds show variable flow directions, mainly towards the S, with variations to the SE, SW, and even to the N or E. The upper half of the succession is interpreted as deposited in distal lakes or lagoons; the lower half of the deposit can be related to abandoned channel or floodplain deposits. The recognition of a large amount of glass shards is interpreted as derived from distal volcanism.

4.1.11. Stratigraphic relations and facies associations

Fieldwork and mapping of the recognized facies (Fig. 2) suggest that the columnar jointed andesite of Facies 1 and the flow foliated rhyolite of Facies 2 crop out together, but with Facies 2 overlying Facies 1 (Fig. 2). These two facies are emplaced over rocks that are tentatively assigned to the Los Menucos Group, although the contact surface

525 is covered. The attitude of the upper layers suggests the existence of an angular
526 unconformity. The sedimentary and volcaniclastic facies (Facies 5 to 10) comprehend a
527 concordant succession. The massive andesite of Facies 3 is emplaced following an E-W
528 direction, and although the outcrops are not well exposed, the shape of this Facies 3
529 suggests that it was emplaced concordant to the sedimentary succession on the eastern side
530 of the CPG (Fig. 2). Similarly, field relations suggest that the sedimentary and
531 volcaniclastic succession, together with the massive andesite of Facies 3, was emplaced
532 above the volcanic facies 1 and 2; dip and strike of the rocks support the existence of an
533 angular unconformity between the concordant succession and the lower volcanic facies 1
534 and 2.

535 The massive rhyolite dikes of Facies 4 are only intruding the basement rocks
536 of the Colo Niyeu Formation, La Esperanza Complex and Los Menucos Group; no rhyolite
537 dikes were identified intruding the other nine facies described before. In addition, this
538 Facies 4 is following E-W direction, or was emplaced along sigmoidal trends along the
539 extent of the faults of the CPG. This suggests that these dikes were coevally intruded with
540 the development of the faults. The lack of dikes intruding the other facies suggests that
541 Facies 4 constitutes the oldest record related to the CPG fault development. Other rhyolitic
542 dikes are also present in the area. They are cross-cut by those that are here assigned to
543 Facies 4; these earlier dikes are probably related to the La Esperanza Complex (e.g.,
544 Giacosa et al., 2007; Martínez Dopico et al., 2019 and references therein).

545 Regarding the sedimentary and volcaniclastic succession, three facies
546 associations A, B and C are recognized. Facies Association A is given by Facies 6 and 8,
547 and Facies 7 is also present but subordinate. The bottom of this facies association is a major

surface, which sometimes is erosive. This surface indicates the deposition of coarse facies with lobate aspect that is followed by massive sandy deposits. The recognition of Facies 7 is indicative of less dense flows that allowed deposition of tractive-flow dominated deposits. This association is representative of clastic wedges, deposited by alluvial fans on proximal areas. Paleocurrents from Facies 6 indicate that these fans were deposited towards the S, SE and SW.

Facies Association B combines Facies 7, 8 and 9. The base of this association is given by an extensive erosive surface. This surface suggests a change of the depositional system, which is dominated by gravelly channels and overlapped by sandy skirts related to down-slope loss of transport capability. Paleocurrent directions from Facies 9 show a progressive migration to the sides (paleocurrents to SE and SW) and possibly generating transversal, minor, fluvial systems in distal position (paleocurrents to the E and W).

Facies Association C is given by Facies 10, 9, and 5. These deposits represent distal deposits, which are mainly characterized by settling from water bodies and minor, sandy tractive flows. In the lower half of the succession, settling processes can be linked to abandoned channels, swamps, floodplains, or occasionally small lakes. In the upper half, this association might represent lacustrine sedimentation, where distal pyroclastic sediment of Facies 5 was easily preserved.

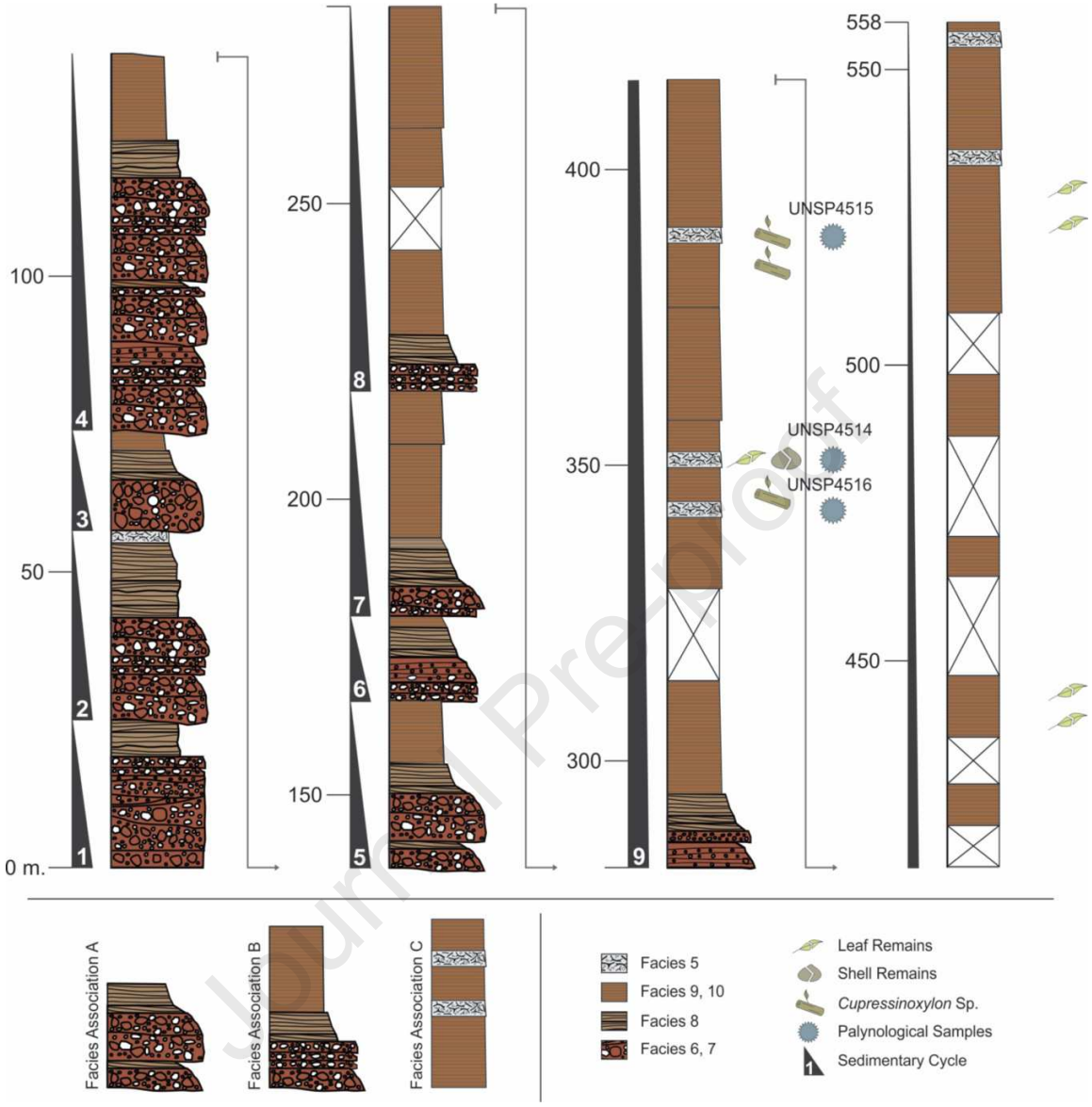

Figure 6. Detailed sedimentary profile measured to the NW of Puesto L. Álvarez. The levels for the three palynological samples are indicated. Based on the sedimentological study, nine sedimentary cycles were recognized; the resulting fining upward arrangement for each cycle is interpreted as a retrogradational stacking pattern. The three schematic facies associations A, B and C are also shown.

4.2. Palynofacies analysis

A statistical count was performed for the two lower samples (Fig. 6), because in the upper one the organic content is so scarce that 500 particles could not be counted. The three studied levels are barren in palynomorphs. The PT-UNSP4514 and PT-UNSP4515 samples are dominated by phytoclasts (87.88–89.2%), mainly by black-brown fragments (48.4–43.8% respectively) (Table 2). The opaque phytoclasts are present in minor proportion (22.28–20%), and in this group the small equidimensional particles are predominant (Fig. 5C-E; Table 2). The amorphous organic matter (AOM) shows similar frequencies in both palynofacies (11.4–10.8%); in PT-UNSP4514 it mainly has a spongy aspect, and in PT-UNSP4515 it is chiefly of fibrous type (Table 2). The scant palynological matter (PM) in the UNSP4516 sample shows a strong degree of degradation (chemical oxidation in the sense of Delcourt and Delcourt, 1980) and is represented by brown particles that are in part structureless (Fig. 5E). In all samples the PM is non-fluorescent.

595 Table 2. Descriptions of dispersed organic components identified in this study; terminology
596 based on Batten (1983), Tyson (1995), and Oboh-Ikuenobe and de Villers (2003).

Main division	Groups of microscopic organic components	Subgroups	Category	Description
Structured palynological organic matter	Phytoclasts (PHY) (woody fragments of land plants)	Translucent (at least at edges)	Cuticle	Particles with different types of "cell" patterns
			Yellow-brown fragment	Particles angular in shape and small in size; without structures
			Black-dark brown fragment	Particles angular in shape and small in size; without structures
			Degraded	Degraded, partially amorphized, macrophyte tissue with irregular or embayed appearance
		Opaque (Oxidized or carbonized woody material)	Lath-shaped	Elongate particles, without structures, variable in size
			Equidimensional	Quadrangular particles, without structures, variable in size
Unstructured organic matter	Amorphous Organic Matter (AOM)		Spongy	Masses with homogeneous aspect, orange-brown to pale or dark brown in color
			Fibrous	Masses with typical internal fibres, orange-brown to pale or dark brown in color

597

598 ***4.3. U-Pb and Lu-Hf analysis (LA-MC-ICP-MS)***

599 Sample GP1 (40°36'39.19"S; 68°22'36.66"W), was collected to the south of
600 Puesto D. Mussi (Fig. 2) for U-Pb zircon provenance analysis and determination of Hf
601 isotope compositions on zircon. This sample corresponds to Facies 10, a massive to fine-

602 laminated mudstone and sandstone (Fig. 4F). The U-Pb analyses involve 101 measurements
603 on 98 zircon crystals. From these analyses, seventy-two were concordant between 90 and
604 110 % (Fig. 7A), considering the relation between the $^{238}U/^{206}Pb$ and $^{235}U/^{207}Pb$ apparent
605 ages. The probability density plot of this dataset (n = 72) delineates a polymodal
606 distribution with three main populations (Fig. 7C). The most abundant one (~54 %) is
607 Jurassic in age with a range between 193 and 173 Ma, the second population (~29 %) is
608 Permian to Early Triassic, with an age range from 293 to 245 Ma, and a small third
609 population (~6 %) is also Triassic, but with strictly Norian ages (210 Ma). The main
610 population of Jurassic age has a youngest graphical peak (YPP, see Sharman and
611 Malkowski, 2020 and references therein) at 185 Ma (Pliensbachian) and a second, less
612 represented population at 191 Ma (Sinemurian). The second population has two important
613 peaks at 264 and 271 Ma. Furthermore, scarce data at 320 Ma, 367 Ma, 470 Ma, 532 Ma,
614 551 Ma, 645 Ma and 1330 Ma were also obtained.

615 The zircon crystals of the main population that delineates the YPP at 185 Ma
616 (n= 28) are prismatic and bipyramidal with magmatic zonation (Fig. 7A – inset). The 28
617 crystals yielded a weighted average age of 183 ± 2 Ma (MSWD = 2.27), which is
618 interpreted as the maximum depositional age (MDA) for the massive to fine-laminated
619 mudstone and sandstone of Facies 10. The oldest crystals of this population, related to the
620 191 Ma peak, have sub-rounded to prismatic shapes (Fig. 7A – inset). Furthermore, the
621 Th/U ratios for both populations are higher than 0.2, indicating igneous origin.

622 Lu-Hf isotope analyses on zircon from the main population (between 192
623 and 183 Ma) show negative to positive ε_{Hf} values of -5.7 and +1 and Mesoproterozoic T_{DM}
624 of 1.5–1.1 Ga. Permian to Triassic crystals (between 270 and 210 Ma) have more negative

625 ε_{Hf} values between -36 and -6.5 and Archean to Paleoproterozoic T_{DM} of 3.4–1.6 Ga. One

626 crystal dated to 532 Ma has an $\varepsilon_{Hf\,(T)}$ of -4.5 and Paleoproterozoic T_{DM} of 1.7 Ga.

627

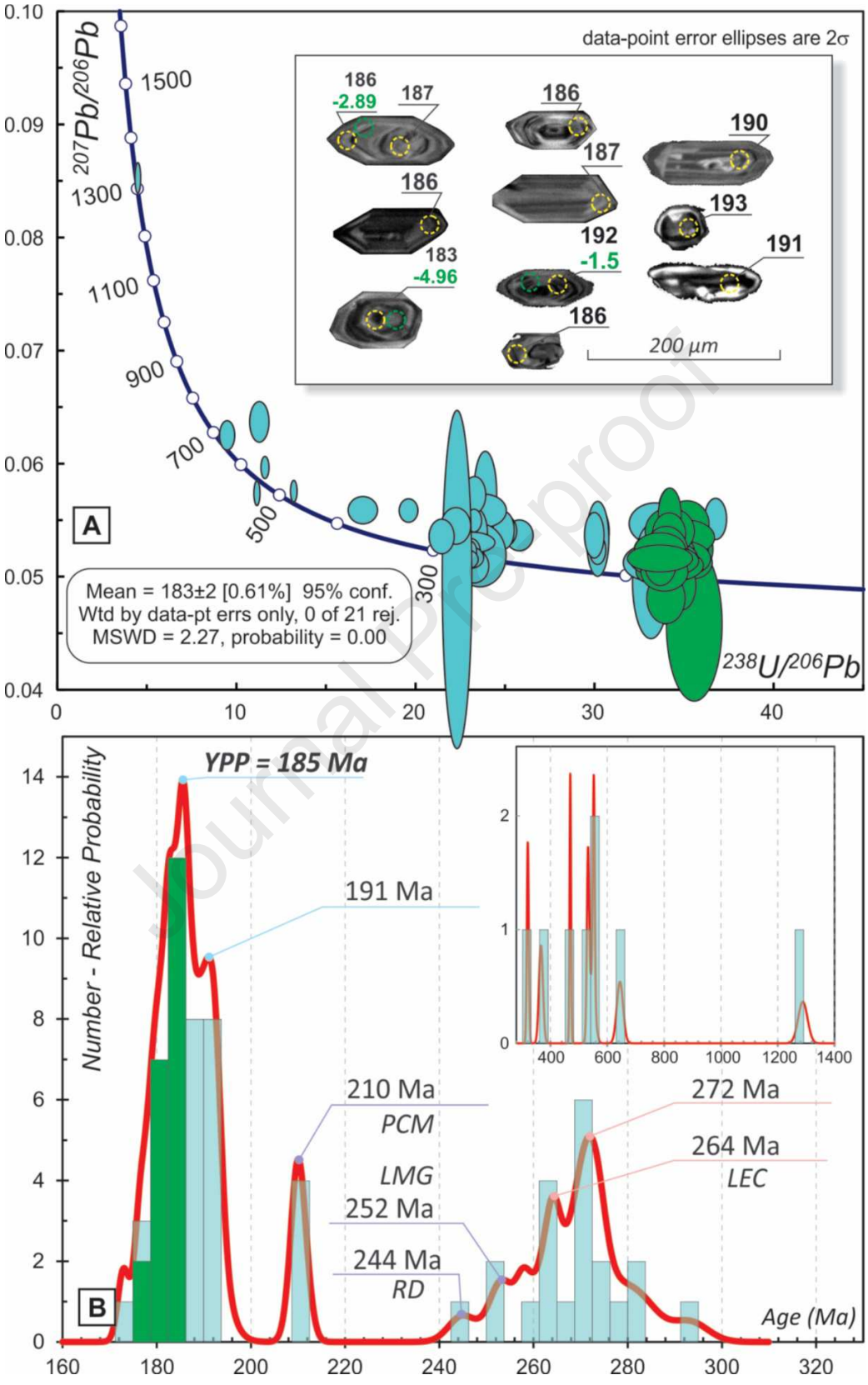

628

Figure 7. U-Pb isotope analysis of sample GP1. (A) Tera-Wasserburg concordia diagram showing the distribution of the most concordant data. The inset shows representative zircon morphology: in black the $^{206}Pb/^{238}U$ ages, and in green the ε_{Hf} values. The error quoted is the realistic error; it was based on the quadratic addition of the average mean error (given by Isoplot) and the 1% error representing the inherent precision of the technique. (B) Probability density plot showing the $^{238}U/^{206}Pb$ U-Pb age distribution of the youngest and most abundant populations of the analyzed crystals. The inset shows the oldest single ages. PCM: Puesto Cuya Monzonite, RD: Rhyolitic dikes, LMG: Los Menucos Group, LEC: La Esperanza Complex. YPP is the youngest graphical peak, that was calculated taking into account the youngest mode in the probability density plot following Couts et al. (2019).

5. Discussion

5.1. Stratigraphy and sedimentology

Based on the field relations between facies described in Section 4.1.11, we propose the existence of an intrabasinal angular unconformity. Thus, the entire volcanic and sedimentary sequence restricted to the CPG is divided into a lower and an upper section. The lower section is composed of the columnar jointed andesite of Facies 1 and the flow-foliated rhyolite of Facies 2, recognized in the eastern part of the study area, close to Puesto D. Mussi and Puesto J. Velo (Fig. 2). The upper section, unconformably deposited over the lower one, is composed of all the other sedimentary and volcaniclastic facies (Facies 5 to 10) and the massive andesite of Facies 3. The upper section is better exposed in the western part of the study area, to the north of Puesto L. Álvarez. Other minor exposures were

651 recognized on the eastern side of the graben, where the angular unconformity between the
652 lower and upper sections was recognized. This difference between the exposures of the
653 eastern and western sidesof the tectonic structure could be the result of different rates of
654 subsidence along the basin. This feature is consistent with a pull-apart type basin proposed
655 by Giacosa et al. (2007), in which different parts of the basin exhibit differential subsidence
656 and, therefore, different accommodation space.

657 The massive rhyolitic dikes of Facies 4 cannot be spatially linked to the two
658 sections mentioned above. These dikes are only intruded into the basement rocks of the
659 CPG, like the La Esperanza Complex, Colo Niyeu Formation, or Los Menucos Group.
660 Therefore, these massive rhyolitic dikes can be tentatively linked to the initial stage of the
661 development of the tectonic depression, contemporaneous to the lower section or even
662 slightly older.

663

664 *5.1.1. Sedimentary depositional model for the upper section*

665 Three facies associations were recognized based on field observations. These
666 associations are here interpreted as representative of proximal (Facies association A - FA),
667 medial (Facies association B - FB), and distal parts (Facies association C - FC) of the
668 downslope evolution of an alluvial fan (Fig. 8). The FA represents the initial stage of the
669 fan. The rapid generation of coarser facies deposited by debris flows represents clastic basal
670 wedges, in response to the rapid generation of accommodation space caused by the
671 development of the tectonic depression.

672 FB and FC represent the medial and distal portions of the fan, respectively,
673 indicating the progressive infill of the depression with finer sediments. The finer sediments
674 can be derived either as continuous sedimentary input to the depression, mostly from the
675 north, or by reworking of the lower facies as suggested by the strong degree of degradation
676 or chemical oxidation of the palynological samples (see Section 5.2). In addition, a distal
677 volcanic provenance should be considered, which would be the source of the glass shards
678 recognized in Facies 10 and the ash fall deposits of Facies 5. The transition between the
679 proximal and medial sections is characterized by amalgamated gravelly to coarse-sandy
680 channels. Decrease of clast size is related with shallower channels and overbank sandy
681 deposits (sandy skirts), possibly related to the stabilization of the slope.

682 The distal portion, represented by FC, is characterized by fine-grained
683 deposits, which are dominated by mudstone. These deposits are massive to fine laminated.
684 Sandy interbeds are scarce and there are small current or symmetrical ripples. Another
685 feature is the presence of biological activity represented by shell and leaves imprints. In the
686 lower part of the succession, this FC is interpreted as abandoned channels or swamps, and
687 in the upper part, it would represent lakes or lagoons.

688 The vertical stacking of the two or three facies associations conforms to an
689 individual sedimentary cycle, with each sedimentary cycle fining-upward and bounded at
690 the bottom and at the top by a major surface that occasionally can be erosive. In the study
691 profile, nine cycles were recognized and all are composed of proximal to medial and/or
692 distal deposits (Fig. 6). The recognized cyclicity could be tentatively linked to fault
693 reactivation, which would be responsible for the rejuvenation and subsequent deposition of
694 the following sedimentary cycle (e.g. Heward, 1978).

Cycles 1 to 6 are dominated by proximal to medial deposits, with minor distal deposits at the top; these cycles are representative of the first stages of basin development and sedimentary infill (Fig. 8). Distal facies is scarcely developed and restricted to abandoned channels or local swamps developed on the floodplain. The poorly developed medial deposits of these cycles evidence a rapid transition from proximal to distal facies caused by a steep fan surface.

Cycles 6 to 9 are progressively dominated by medial to distal facies, indicating minor tectonic activity and fine sediment supply. The thickness of distal facies in these cycles is at the scale of tens of meters - indicative of lacustrine sedimentation and a shallow fan surface. The progressive diminution in thickness of proximal facies and increase of distal facies can be related with progressive retraction of the fault scarp, which results in a retrogradational configuration (Fig. 8).

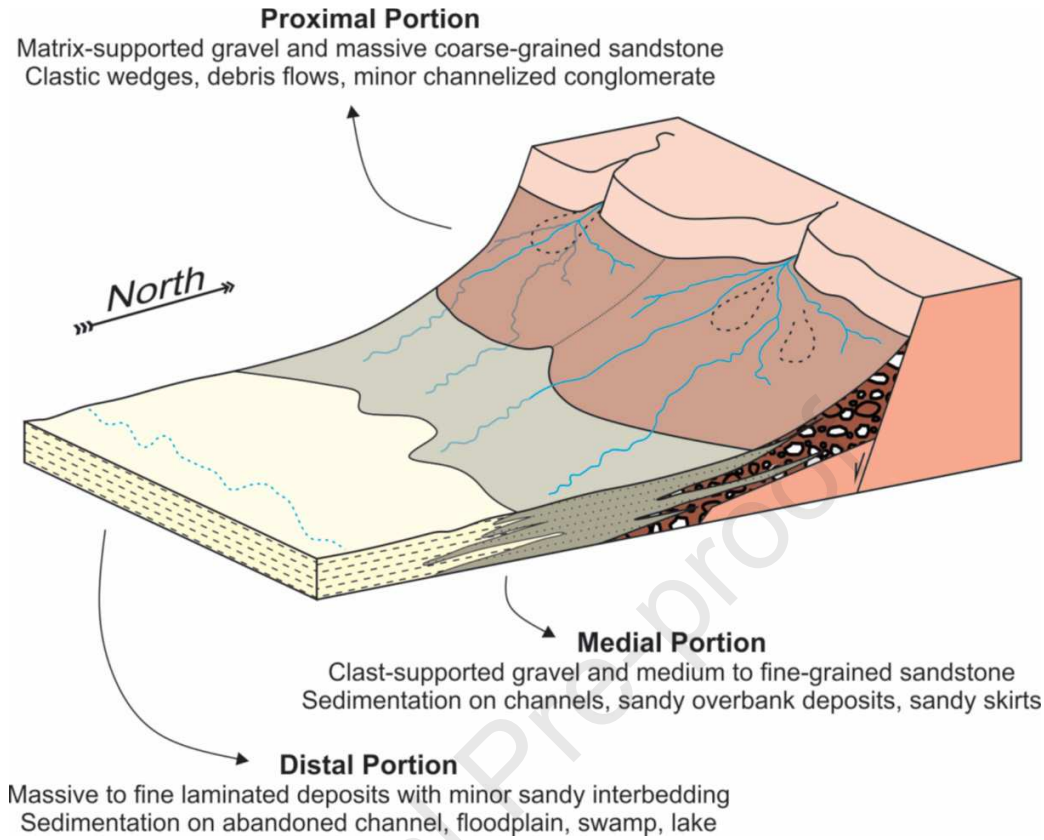

Figure 8. Simplified sketch for the sediment deposits in the Cerro Piche graben based on facies analysis. Three main portions were identified based on facies associations, which suggest an alluvial depositional environment. A brief description of the three portions of the downslope evolution of the alluvial fan is provided in the text.

5.2. Palynological interpretation

The composition and distribution of the dispersed microscopic organic components (i.e., palynomorphs, fungal remains, plant debris, and AOM) in sedimentary rocks reflect their taphonomic history (e.g., distances and/or time of transport, sorting, burial conditions, and post-depositional changes) and the biosphere association from which

719 the palynological fossils were derived. As mentioned above, the study of a clastic deposit
720 from a palynological point of view constitutes a useful tool to elucidate the depositional
721 conditions of the sediments carrying palynological matter (e.g., Tyson, 1995; Oboh-
722 Ikuenobe and de Villers, 2003).

723 The three studied samples, related to ash-fall deposits accumulated in water
724 bodies (Facies 5), show a large percentage of land plant debris that suggests an important
725 terrestrial input into this depocenter. High frequencies of dark brown and opaque
726 phytoclasts, such as those recognized in these Palynofacies Types (Fig. 5C-D), were
727 interpreted by Oboh-Ikuenobe and de Villers (2003) as a consequence of a relatively high
728 degree of oxidation at the source of the phytoclasts, prior to deposition. However, if the
729 dark-colored phytoclasts present fairly rounded edges, these authors suggested that the
730 particles may have been either recycled from older deposits or transported far from their
731 source before deposition. Furthermore, Tyson (1995) pointed out that among the opaque
732 phytoclasts, the predominance of equidimensional, relatively smaller particles, rather than
733 lath-shaped ones, could be the result of long distance transport from the source area. The
734 recognized Palynofacies Types, namely dark particles with angular and rounded edges (Fig.
735 5D), degraded phytoclasts, and scarce non-fluorescence AOM (Fig. 5C-D), reflect a high
736 degree of oxidation under environmental conditions in which other components have been
737 selectively destroyed (Tyson, 1995). The scant palynological matter identified in the
738 UNSP4516 level, only composed of degraded tissues, reinforces this idea (Fig. 5E). This
739 strong chemical oxidation could reflect the intermittent exposure to weathering and/or
740 intense reworking. The presence in Facies 5 of rounded lithic clasts related to a local
741 epiclastic input suggests that these sediments, and the associated organic components,

742 could have been the result of a dynamic system with high terrestrial input, sediment
743 reworking, and/or intermittent subaerial exposure.

744

745 ***5.3. Paleofloristic content***

746 The first mention of a fossil plant from the Cerro Piche succession was made
747 by Labudia et al. (1992), who described two specimens of stem impressions assigned to the
748 lycophyte *Pleuromeia* sp. The same authors found a second plant fossil, a stem impression
749 and a stem permineralization (not published – collection of the Museo de La Plata,
750 Argentina) that they also assigned, although with doubts, to *Pleuromeia* sp. These fossil
751 plants were later reinterpreted by Coturel (Museo de La Plata - Argentina, pers. commun.)
752 and Bodnar and Falco (2018) as conifer material.

753 Recently, Bodnar and Falco (2018) described four samples of permineralized
754 trunks and branches, of 5–23 cm diameters, from Facies 5 (Fig. 5). These materials
755 correspond to the conifer genus *Cupressinoxylon*, but their regular preservation prevented
756 their assignment at the species level. The size of the sample, added to the presence of
757 branch traces and scars, indicates that the plants had a profusely branched tree-habit. The
758 genus *Cupressinoxylon*, related to the Cupressaceae family, had a wide distribution
759 extending throughout both hemispheres in the Upper Triassic to Miocene (Philippe et al.,
760 2004; Gnaedinger and Zavattieri, 2020); consequently, its detection would not provide
761 conclusive information about the age of these strata.

In summary, the paleoflora preserved in the sedimentary succession of the Cerro Piche Graben is, until now, composed exclusively of conifer material, and probably corresponds to an arboreal paleocommunity.

5.4. U-Pb maximum depositional age (MDA) versus true depositional age (TDA)

It has been discussed over recent years how to best determine the maximum depositional age (MDA) of a detrital sample on the basis of U-Pb on zircon, and whether this MDA can be considered to reflect the true depositional age (TDA) (e.g., Dickinson and Gehrels, 2009; Couts et al., 2019; Sharman and Malkowski, 2020, among others). Dickinson and Gehrels (2009) supported the use of the youngest U–Pb ages for individual detrital zircon grains to constrain the MDA.

Couts et al. (2019) concluded that no single MDA method is the most successful in constraining the MDA, however, these authors emphasized that better calculations can be derived from large datasets of high precision ages. They also discussed that the most used methods for MDA determination have been to use; i) the youngest single grain (n = 1), ii) the youngest grain cluster at 2σ uncertainty (n > 3), which is calculated by computing the weighted average age of the youngest three or more dates that overlap within 2σ uncertainty, and iii) the youngest graphical peak (YPP) that is calculated from the age of the youngest mode in the probability density plot of the measured sample (n > 1).

Sharman and Malkowski (2020) suggested, for ancient detrital samples, the use of one or more conservative MDA methods based on multiple, overlapping age measurements to reduce the risk of calculating an MDA that is younger than the TDA, which could result from late resetting of the U-Pb isotopic pair. Based on these ideas, we

use the YPP method to constrain the youngest and well represented population, which in turn involves the largest dataset; and we finally use a weighted average age involving the most concordant data of the YPP to calculate the MDA (Fig. 7).

U-Pb isotope analysis on zircon grains from sample GP1 gave a YPP (~54 %) of 185 Ma (Pliensbachian) and a weighted average age of 183 ± 2 Ma that is interpreted as the MDA (Fig. 7). A significant percentage of glass shards found in Facies 10 and the prismatic shapes of zircon crystals (with magmatic zonation) could be indicative of a distal volcanic source, probably outside of the graben. Then, the possible source for these zircons may have been the coeval magmatism related to the Subcordilleran Patagonian Batholith located to the south-west of the study area, which has been dated between 181 and 185 Ma (Rapela et al., 2005). If this is indeed the correct source, sedimentation would have been synchronous with distal volcanism (Fig. 9), and the ca. 183 Ma age could represent the true depositional age (TDA) of Facies 10 at the CPG. To consider that the analyzed deposit yielded an MDA close to the TDA, the two fundamental requirements (Sharman and Malkowski, 2020; see also Rossignol et al., 2019) would be fulfilled: the first that there must be a source of contemporaneous grains, in this case the Subcordilleran Patagonian Batholith, and the second that the supply from that source is much higher with respect to the supply of older sediment sources (the youngest population representing ~54% for the total amount).

Besides the youngest population, we identified a peak with an age of ca. 191 Ma (Sinemurian). The possible source for grains with this Sinemurian age could be the Comallo Complex (Barros et al., 2020) to the west, or the Subcordilleran Patagonian Batholith (Rolando et al., 2002) to the southwest of the study area. Another possible source

for the Sinemurian zircons could be the Marifil Volcanic Complex east of the CPG, with U-Pb zircon ages between 190 and 193 Ma (Strazzere et al., 2018; Pavon Pivetta et al., 2019).

Late Paleozoic to early Mesozoic ages are correlative with those presented by Lema et al. (2008), Luppo et al. (2017, 2019), and Martínez Dopico et al. (2017, 2019). The age of ca. 210 Ma (Fig. 7) could be related to the monzogranite of Puesto Cuya dated to ca. 207 Ma (^{40}Ar-^{39}Ar on biotite - Lema et al., 2008). The Middle Triassic ages correspond to a rhyolitic dike swarm formed at ca. 244 Ma (Luppo et al., 2019, and references therein); and Early Triassic ages could be related to the Los Menucos Group developed around 253 to 248 Ma (Falco et al., 2020). Finally, Permian ages are correlative with that of the La Esperanza Complex (Luppo et al., 2017, 2019; Martínez Dopico et al., 2017, 2019, and references therein). The oldest and not abundant ages are consistent with the results of provenance analysis for the metamorphic basement of the Colo Niyeu Formation (Martínez Dopico et al., 2017; Chernicoff et al., 2018).

Our U-Pb MDA of 185 Ma discards the initially proposed Triassic age for the CPG that was based on the paleontological record (see Labudia and Bjerg, 2001), and supports an Early Jurassic depositional age for the CPG sedimentary sequence, as previously suggested by Bodnar and Falco (2018).

5.4.1. The Early Jurassic U-Pb age record for northern Patagonia

The Pliensbachian provenance age obtained for the CPG, which is assumed to be the TDA, allows us to correlate it with ages of other units in the North Patagonian Massif (NPM) (Fig. 9). To the west of the NPM, the Garamilla and Taquetrén formations have been dated to the Pliensbachian (Franzese et al., 2002; Benedini et al., 2014, 2020).

To the east of the NPM, the El Sotano granodiorite and the Marifil Volcanic Complex also have Pliensbachian ages (Sato et al., 2004; Pavon Pivetta et al., 2019 and references therein). To the south of the NPM, into the Cañadón Asfalto Basin, Pliensbachian ages were also obtained for the lower Las Leoneras Formation (Cúneo et al., 2013).

Tectonic studies carried out on the CPG by Giacosa et al. (2007) suggested that the extensional tectonics that led to the opening of this tectonic depression were NE to NNE oriented. With the new Pliensbachian provenance age for the CPG we can now propose that this NE directed stress field is of Early Jurassic age. A similar tectonic pattern was also recognized for the Marifil Formation for Sinemurian to Pliensbachian times (Strazzere et al., 2018; Pavon Pivetta et al., 2019). Pavon Pivetta et al. (2019) described an angular unconformity between two different successions assigned to the Marifil Formation - the lower succession of Sinemurian age, and the upper with a Pliensbachian age. Based on these comparisons, we suggest that the CPG might have been developed since the Sinemurian, and the unconformity between the lower volcanic and the upper volcanic and sedimentary sections in the CPG might reflect the same tectonic episode described for the Marifil Formation.

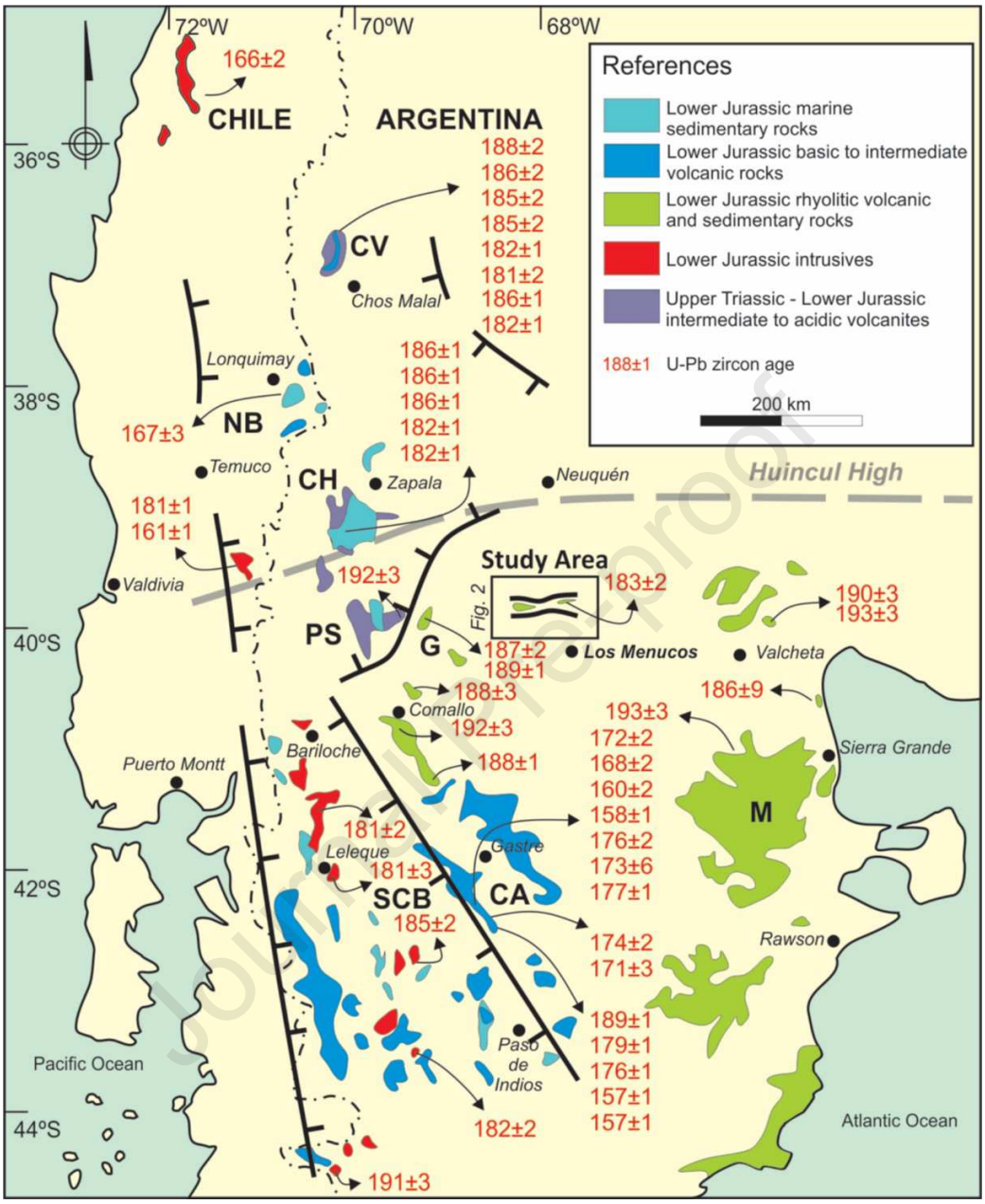

Figure 9. Simplified geological map with Lower Jurassic igneous and sedimentary units in Patagonia, modified after Naipauer et al. (2018) and Rossel et al. (2020). M: Marifil Complex; CA: Cañadón Asfalto Basin including the Lonco Trapial Formation; SCB: Subcordilleran Patagonian Batholith; G: Garamilla Formation including the Comallo and Cañadón Chileno complexes; PS: Piedra del Águila and Sañicó formations; NB: Nacientes

del Río Biobío Formation; CV: Cordillera del Viento, CH: Chachil Limestone. Ages for the Marifil Complex after Sato et al. (2004), Strazzere et al. (2017, 2018), and Pavon Pivetta et al. (2019); Garamilla Complex after Franzese et al. (2002) and Benedini et al. (2014); Comallo Complex after Barros et al. (2020); Cañadón Chileno Complex after Benedini et al. (2020); Cordillera del Viento after Leanza et al. (2013) and Zappettini et al. (2018); Chachil Limestone after Leanza et al. (2013) and Armell et al. (2016); Subcordilleran Patagonian Batholith after Rolando et al. (2002) and Rapela et al. (2005); Cañadón Asfalto Basin and Lonco Trapial Formation after Cúneo et al. (2017), Bohuier et al. (2017), Hauser et al. (2017) and Zaffarana et al. (2020); Nacientes del Biobío Formation after Rossel et al. (2020) and references therein.

5.5. Stratigraphic proposal

The new data presented in this manuscript allow us to define the Cerro Piche Formation, a new Lower Jurassic unit in the central North Patagonian Massif (Fig. 2). The Cerro Piche Formation is the only stratigraphic unit inside the Cerro Piche Graben (Corbella, 1973). It overlies the Colo Niyeu Formation, the La Esperanza Complex, and the Los Menucos Group. According to Giacosa et al. (2007), the basin development was triggered by NE extensional tectonics, which in turn triggered the infilling of the tectonic depression.

Based on field observations, we propose to divide the Cerro Piche Formation into the lower Loma Blanca Member (modified after Cucchi et al., 2001) and the upper El Tono Member, which are separated by an intrabasinal angular unconformity. The *Loma*

876 *Blanca Member* crops out in the eastern part of the graben and corresponds to the andesite
877 and rhyolite lavas of Facies 1 and 2; this member represents the initial stage of basin
878 development, tentatively assigned to the Sinemurian. The *El Tono Member* crops out along
879 the graben with better exposures in the western part, and includes the massive andesite of
880 Facies 3 and the sedimentary succession that represents the infill of the tectonic depression
881 from Pliensbachian time. Sedimentary facies analysis carried out on the El Tono Member
882 suggests that sedimentation occurred in alluvial fans, in which fossil trunks assigned to
883 *Cupressinoxylon* sp. (Bodnar and Falco, 2018) were identified, as well as palynological
884 matter with a high degree of deterioration; shell and leaf imprints were also mentioned from
885 the basin (Corbella, 1973, this study).

886

887 ***5.6. Hf isotope data from detrital zircon from the CPG: combining provenance and***
888 ***crustal evolution***

889 *5.6.1. U-Pb and Hf combined provenance analysis*

890 Our Hf isotope analyses show similarities with previous studies in the NPM.
891 The combined U-Pb and Hf isotope analysis is a powerful tool to establish provenance and
892 to identify the possible source(s) for the studied deposit (e.g., Gehrels, 2014). In our CPG
893 analysis, one zircon crystal dated to 532 Ma has $\varepsilon_{Hf\,(T)}$ of -4.5 and Paleoproterozoic T_{DM} of
894 1.7 Ga suggesting a source derived from a recycled continental crust. Similar Hf isotope
895 values were obtained in Cambrian plutons in the eastern part of the NPM (see Rapela and
896 Pankhurst, 2020).

The Permian-Triassic zircons of the CPG suggest that these crystals are derived from a source in which the main process of magma generation was the recycling of continental crust. The $\varepsilon_{Hf(T)}$ values of the zircon crystals of sample GP1 vary between -36 and -6.5, and the recycled crust was Archean to Paleoproterozoic, with T_{DM} of 3.4-1.6 Ga. These values agree with previous Hf isotope studies carried out on Permian-Triassic magmatic rocks (Chernicoff et al., 2013; Castillo et al., 2017). In addition, and based on the observed paleocurrent directions, the most plausible source for these zircons is the La Esperanza Complex, which is part of the basement in the CPG region and crops out immediately to the north of the graben (Fig. 2).

The negative to positive $\varepsilon_{Hf(T)}$ values from -5 to +1 found in the Jurassic zircon grains, related with the maximum depositional age of 185 Mas, indicate that the main processes related to the generation of these zircons in the source areas could have been: i) partial melting of a Mesoproterozoic lower crust (T_{DM} of 1.5-1.1 Ga), ii) or a fossilized lithospheric mantle (Pankhurst et al., 2000; Hauser et al., 2017), or iii) a juvenile magma source that had been contaminated with Mesoproterozoic crust (T_{DM} between 1.5 and 1.1 Ga). The Hf isotopic compositions of zircons from the CPG (Fig. 10) are similar to the values for zircon from the Cañadón Asfalto Basin (Hauser et al., 2017). Thus, the negative and positive $\varepsilon_{Hf(T)}$ values of the CPG could be consistent with a reworked crustal source with a possible minor contribution of juvenile magma.

The U-Pb and Hf combined analysis also suggests that different stratigraphic units of the NPM likely contributed as sources for the CPG detritus. Populations of zircon with ages older than Jurassic are mainly derived from the north and east, whereas the Jurassic sources can be related to distal volcanism (ash fall), possibly the Jurassic

magmatism of the western part of the NPM. On the other hand, and although there are no available analyses for comparison, the magmatism of the Marifil Volcanic Complex cannot be discarded as a possible source.

5.6.2. Crustal evolution of the North Patagonian Massif during Jurassic times

Hauser et al. (2017) reported a Hf isotope study on zircon from the Cañadón Asfalto Basin. They described the Cañadón Asfalto magmatic event in terms of three major cycles: C1, C2 and C3 (Fig. 10).

The *C1 Lonco Trapial* (172-180 Ma) cycle, which is characterized by a prominent peak at 176 Ma, is well constrained by Hf isotopic compositions on zircon showing negative and positive $\varepsilon_{Hf(T)}$ values between -2.2 and +4.0. These values suggest that these magmas could have either been generated by juvenile magmas strongly contaminated with old crust, or by partial melting of old lower crust or fossilized lithospheric mantle, of Neoproterozoic-Mesoproterozoic age (~1.0 Ga). Part of the data presented in this study for the CPG are consistent with this C1 (Fig. 10).

The *C2 Las Chacritas* (166-169 Ma) magmatic cycle is well constrained by Hf isotopic compositions of zircon crystals - with negative $\varepsilon_{Hf(T)}$ values. This magmatism represents crustal reworking during Jurassic times of an old crust with T_{DM} between 1.4 and 1.55 Ga, which is also similar in terms of Hf isotopic character to the Mamil Choique magmatic event (see Hauser et al., 2017). They interpreted that it was possible that Mamil Choique basement was recycled at ~168 Ma during C2.

941 The last magmatic cycle *C3 Puesto Almada* (155-162 Ma) shows mixed Hf
942 isotope characteristics, from negative to slightly positive $\varepsilon_{Hf(T)}$ values between -5.6 and 2.1
943 and T_{DM} between 1.3 and 0.9 Ga. This magmatic cycle was interpreted to represent a
944 juvenile magma that was highly contaminated with old crust.

945 The new data provided in the present study suggest the occurrence of an
946 older C0 magmatic cycle, with Hf isotope character comparable to C3 of Hauser et al.
947 (2017). Similarly, some of the data previously presented by Hauser et al. (2017) also
948 suggest the existence of another source for the C1 cycle, here denoted as $C1_i$, that is
949 contemporaneous to C1, but has a Hf isotope signature similar to C2.

950 The *C0* magmatic cycle is constrained between 182 and 192 Ma, with a
951 prominent peak at 185. For C3, the $\varepsilon_{Hf(T)}$ values suggest a mixed isotopic character, with
952 values between -8 and +1, and Mesoproterozoic T_{DM} of 1.5–1.1 Ga. As discussed before,
953 this isotopic character can be interpreted in terms of mixed sources, dominated by crustal
954 reworking and scarce juvenile contributions, although the source area is still unknown.

955 The $C1_i$ source is part of the C1 cycle (172-180 Ma) of Hauser et al. (2017).
956 The $\varepsilon_{Hf(T)}$ values suggest crustal reworking, as interpreted for C2 by Hauser et al. (2017).
957 This new proposal highlights that during the 172–180 Ma interval there were two different
958 Hf isotopic sources, one related to C1 (after Hauser et al., 2017) that most probably reflect
959 a juvenile magma contaminated with a Neo- to Paleoproterozoic crust, and a second source
960 related to $C1_i$ that is interpreted as having been derived from crustal reworking.

961 Recently, Zaffarana et al (2020), based on whole-rock geochemistry and Sr-
962 Nd isotopes, suggested that the Lonco Trapial magmatism of the central NPM had mixed

963 signature between mantle-derived magmas and the lower crust. The Marifil volcanism,
964 developed in the eastern NPM, was chemically related to a thicker crust, with magmas
965 isotopically akin to upper crust. In turn, the Jurassic magmatism of the eastern NPM has
966 more isotopic affinity to mantle-derived magmas (Zaffarana et al., 2020). Based on these
967 new insights about Jurassic magmatism in the NPM, the mixed Hf isotopic values for the
968 C0, C1 and C3 magmatic cycles can be tentatively related to the magmatism developed in
969 the central and eastern NPM, whereas the Hf isotopic signatures related to crustal
970 reworking ($C1_i$ and C2 magmatic cycles) could be related to the magmatism in the western
971 NPM.

972

973 *5.6.3. Relationship between the C0-C3 magmatic events and the putative V0-V3 volcanic*
974 *cycles of Patagonia*

975 Based on geochronological data, Pankhurst et al. (2000, Fig. 10) proposed
976 three main volcanic cycles: V1 (188-178 Ma), V2 (176-162 Ma), and V3 (157-153 Ma).
977 Recently, Pavon Pivetta et al. (2019) suggested that Marifil volcanism is older than 188 Ma
978 and took place during Sinemurian times of ca. 190-193 Ma. Furthermore, these authors also
979 proposed a V0 volcanic cycle based on the recognition of an angular unconformity and
980 geochemical changes within the volcanic strata above. Pavon Pivetta et al. (2019) proposed
981 that V0 had Sinemurian age, with a lower boundary of the V1 cycle related to the
982 Pliensbachian.

983 When the V0-V3 volcanic cycles are contrasted with our Hf-based C0-C3
984 magmatic cycles, some temporal similarities are recognized (Fig. 10). The V0 and V1

985 volcanic cycles seem to be coincident with C0 as proposed here. The probability density
986 curve (Fig. 10) highlights a prominent peak at ca. 185 Ma and a minor peak at 192 Ma,
987 coincident with the unconformity recognized by Pavon Pivetta et al. (2019). The V2
988 volcanic cycle is partially coincident with the C1-C2 events, which begins with a prominent
989 peak at ca. 178 Ma and a minor one at ca. 166 Ma (Hauser et al., 2017). The V3 cycle is
990 marginally coincident with the C3 event (Hauser et al., 2017). It is worthwhile noting that
991 the C0-C3 cycles (Hauser et al., 2017; this study) were defined based on U-Pb and Hf
992 isotope signatures of magmatism exclusively developed in the NPM. Further investigations
993 in different Jurassic units of Patagonia will contribute to a better characterization of the
994 magmatism, Patagonian crustal evolution, and the detrital sources for the Jurassic basins.

995

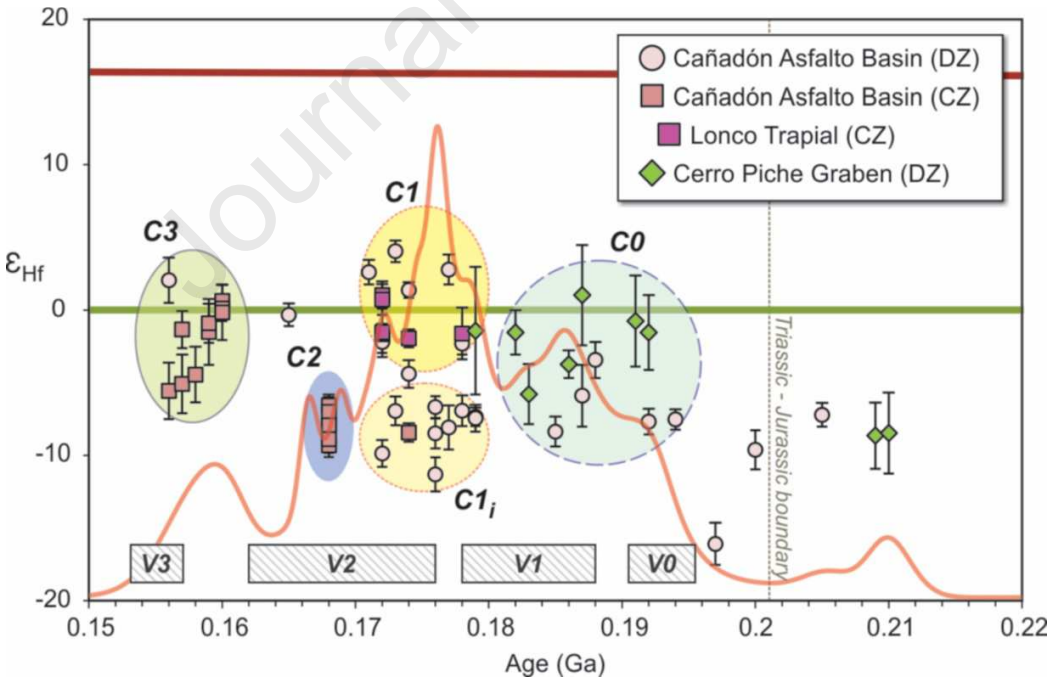

996

997 Figure 10. ε_{Hf} vs Age diagram for the data from the Cerro Piche Graben and Cañadón
998 Asfalto Basin where the C1: Lonco Trapial, C2: Las Chacritas and C3: Puesto Almada

cycles were defined (Hauser et al., 2017). The C0-C3 magmatic cycles discussed in this study are shown (see text for a detailed discussion), based on analysis by Hauser et al. (2017). The V0-V3 volcanic phases of Patagonia correspond to the proposals by Pankhurst et al. (2000) and Pavon Pivetta et al. (2019). Part of the Cañadón Asfalto Basin data are from volcanic rocks (CZ); the remaining analyses from this basin were performed on detrital zircon (DZ). The red lines represent the probability density plot of the detrital zircons of the CPG and the analyses presented by Hauser et al. (2017) for the Cañadón Asfalto Basin. The crustal evolution trends represent the bulk-rock trends for Mesoproterozoic juvenile crust, calculated using the 176Lu/177Hf ratio of 0.0113 (Taylor and McLennan, 1985; Wedepohl, 1995).

6. Conclusions

The Cerro Piche Graben represents an extensional basin in the Central North Patagonian Massif. The graben structure was developed during Early Jurassic times, discarding a Triassic age. The new results of the present work allow defining the Cerro Piche Formation, which is here divided into a lower Loma Blanca Member and upper El Tono Member. The Loma Blanca Member is restricted to the eastern side of the area, and we grouped andesites and rhyolites lavas into this unit.

The El Tono Member crops out along the graben and includes the sedimentary succession that represents the infill of the tectonic depression during the Pliensbachian (ca. 183 Ma), and a concordant andesite lava. Sedimentary facies analysis of the El Tono Member indicates that deposition took place in alluvial fans. The proximal fan

was dominated by mantled gravelly deposits, the medial fan by channelized gravel and sandstone deposits, and the distal fan by lacustrine deposits. Nine sedimentary cycles were recognized in a retrogradational arrangement, with deposition controlled by normal faulting. The palynological matter (PM) recovered from deposits of the El Tono Member is dominated by terrigenous materials, suggesting a high terrestrial input mainly by runoff into the depocenter. The great degree of deterioration of the PM would reflect a taphonomic control rather than the origin of sedimentary organic matter (biocenosis), with selective preservation of the most resistant components. Furthermore, the paleoflora preserved in the El Tono Member likely only involves conifers, which corresponds to an arboreal paleocommunity.

A Lu-Hf isotope study on Early Jurassic detrital zircon crystals of the El Tono Member (MDA of 183 Ma) supports a source derived from the reworking of continental crust, with possible minor contribution of juvenile magma. The evolution of the Hf isotopes in the North Patagonian Massif supports the recognition of four magmatic cycles, called C0, C1, $C1_i$, C2 and C3. The C1 (172–180 Ma) and C3 (155–162 Ma) cycles represent a magmatism involving mixed sources, in which a juvenile magma is contaminated by crust. The C0 (182–192 Ma) cycle, which includes the distal volcanism identified in the CPG, the $C1_i$ source (172–180 Ma) and C2 cycle (166–169 Ma) seemingly represent three episodes of crustal reworking.

Appendix A. Supplementary Material

Supplementary material related to this article can be found at

Acknowledgments

This research is part of JIF´s Ph.D. thesis; financial support came from the Consejo Nacional de Investigaciones Científicas y Técnicas (CONICET - Argentina), Universidad Nacional del Sur (Argentina), Instituto Geologico del Sur (CONICET-UNS), and Universidade de Brasilia (Brasil). The authors are very grateful to Laureano Alvarez, Julio Velo, Domingo Mussi and Napoleon Haunchequeo to cooperate with this research and allowing the fieldwork. JIF especially thanks to Julieta Cresevic, Sala de Becarios UNS, Alberto Fidalgo Castro and Eudes de Oliveira Bomfim for personal support; and colleagues from the Laboratory of Geochronology of the Universidade de Brasilia for analytical support and discussion of the results. NH and WUR have been supported by Brazilian National Council for Scientific and Technological Development (CNPq) fellowships (grants 309878/2019-5 and 305761/2019-6 respectively). We are also grateful for partial support of this study from the Coordenação de Aperfeiçoamento de Pessoal de Nível Superior – Brazil (CAPES) – under Finance Code 001. A detailed critique of this manuscript was made by Dr. C. Navarrete and Dr. S. González, which highly improved its quality; both reviewers and the Managing Guest Editor (Dr. D. Kietzmann) are gratefully acknowledged.

References

1063 Albarède, F., Telouk, S. Blichert-Toft, J., Boyet, M., Agranier, A., Nelson, B., 2004.
1064 Precise and accurate isotopic measurements using multiple-collector ICPMS. Geochimica
1065 et Cosmochimica Acta 68, 2725-2744.

1066 Armell, C., Leanza, H., Corfu, F., 2016. Synsedimentary ash rains and paleoenvironmental
1067 conditions during the deposition of the Chachil Formation (Pliensbachian) at its type
1068 locality, Neuquén Basin, Argentina. Journal of South American Earth Science 71, 82-95.

1069 Asiain L.M., Gargiulo, M.F., Bjerg, E.A., Ntaflos, T., Reitinger, J., 2019. Petrografía y
1070 geoquímica de traquibasaltos y traquiandesitas basálticas de las Vulcanitas Corona Chico y
1071 del Complejo Volcánico Barril Niyeu, noroeste de la Meseta de Somuncurá, provincia de
1072 Río Negro. Revista de la Asociación Geológica Argentina 76(1), 8-23.

1073 Barros, M., Gregori, D., Benedini, L., Paulo, M., Strazzere, L., Pavon Pivetta, C., Geraldes,
1074 M., 2020. Evolution of the Jurassic Comallo volcanic sedimentary complex in the western
1075 North Patagonian Massif, Rio Negro province, Argentina. International Geology Review
1076 DOI: 10.1080/00206814.2020.1731854.

1077 Batten, D.J., 1983. Identification of Amorphous Sedimentary Organic Matter by
1078 Transmitted Light Microscopy. In: Brooks, J. (Ed.), Petroleum geochemistry and
1079 exploration of Europe. Geological Society, Special Publication 11, London, pp. 275–287.

1080 Batten, D.J., 1996. Palynofacies and paleoenvironmental interpretation. In: Jansonius, J.,
1081 McGregor, D.C. (Eds.), Palynology: Principles and Applications. American Association of
1082 Stratigraphic Palynologists Foundation 3, Salt Lake City, USA, 1011–1064.

1083 Benedini, L., Gregori, D., Strazzere, L., Falco, J., Dirstas, J., 2014. Lower Pliensbachian
1084 caldera volcanism in high-obliquity rift systems in the western North Patagonian Massif,
1085 Argentina. Journal of South American Earth Science 56, 1-19.

1086 Benedini, L., Pavon Pivetta, C., Marcos, P., Gregori, D., Barros, M., Scivetti, N., Costa dos
1087 Santos, A., Strazzere L., Geraldes, M., de Queiroz Bernabé, T., 2020. Lower Jurassic felsic
1088 diatreme volcanism recognized in central Patagonia as evidence of along-strike rift
1089 segmentation. Journal of South American Earth Science 106, 102705. DOI:
1090 10.1016/j.jsames.2020.102705

1091 Bodnar, J., Falco, J.I., 2018. Fossil conifer woods from Cerro Piche graben (Triassic-
1092 Jurassic?) North Patagonian Massif, Rio Negro Province, Argentina. Ameghiniana 55(3),
1093 356–362.

1094 Bouhier, V.E., Franchini, M.B., Caffe, P.J., Maydagán, L., Rapela, C.W., Paolini, M.,2017,
1095 Petrogenesis of volcanic rocks that host the world-class Ag\Pb Navidad District, North
1096 Patagonian Massif: comparison with the Jurassic Chon Aike Volcanic Province of
1097 Patagonia, Argentina. Journal of Volcanology and Geothermal Research 338, 101-120.

1098 Brugman, W.A., van Bergen, P.F., Kerp, J.H.F., 1994. A quantitative approach to Triassic
1099 palynology: the Lettenkeuper of the Germanic Basin as an example. In: Traverse A (Ed),
1100 Sedimentation of Organic Particles. Cambridge University Press 19, New York, pp 409-
1101 429.

1102 Castillo, P., Fanning, C.M., Pankhurst, R.J., Hervé, F., Rapela, C.W., 2017. Zircon O- and
1103 Hf-isotope constraints on the genesis and tectonic significance of Permian magmatism in
1104 Patagonia. Journal of the Geological Society 175 (5), 803-816.

1105 Chauvel. C., Blichert-Toft, J.E., 2001. A hafnium isotope and trace element perspective on
1106 melting of the depleted mantle. Earth and Planetary Science Letters 190, 137-151.
1107 Chernicoff, C.J., Zappettini, E.O., Santos, J.O.S., McNaughton, N.J., Belousova, E. 2013.
1108 Combined U–Pb SHRIMP and Hf isotope study of the Late Paleozoic Yaminué Complex,
1109 Río Negro province, Argentina: Implications for the origin and evolution of the Patagonia
1110 composite terrane. Geoscience Frontiers 4, 37–56.

1111 Chernicoff, C., Zappettini, E., Santos, J. 2018. New zircon U-Pb SHRIMP dating of the
1112 Colo Niyeu Formation, Río Negro province, Argentina, and its reassessment as retroarc
1113 foreland metasediments associated with the Devonian-Mississipian west Patagonian
1114 magmatic arc. in: Abstracts Of the XI. South American Symposium on Isotope Geology,
1115 Cochabamba, Bolivia.

1116 Chu, N.C., Taylor, R.N., Chavagnac, V., Nesbitt, R.W., Boella, R.M., Milton, J.A.,
1117 German, C.R., Bayon, G., Burton, K., 2002. Hf isotope ratio analysis using multicollector
1118 inductively coupled plasma mass spectrometry: an evaluation of isobaric interference
1119 corrections. Journal of Analytical Atomic Spectrometry 17, 1567-1574
1120 Cohen, K.M., Finney, S.C., Gibbard, P.L., Fan, J.-X., 2013, updated. The ICS International
1121 chronostratigraphic Chart. Episodes 36, 199-204.
1122 Corbella, H. 1973. Basaltos nefelínicos asociados al graben del cerro Piche, Macizo
1123 Nordpatagónico, provincia de Río Negro, República Argentina. Revista de la Asociación
1124 Geológica Argentina 28(3), 209-218.

1125 Cortés, J., 1981. El sustrato precretácico del extremo nordeste de la provincia del Chubut.
1126 Revista de la Asociación Geológica Argentina 36, 217-235.

1127 Coutts, D.S., Matthews, W.A., Hubbard, S.M., 2019. Assessment of widely used methods
1128 to derive depositional ages from detrital zircon populations. Geoscience Frontiers 10(4),
1129 1421–1435.

1130 Cox, K.G., 1992. Karoo igneous activity, and the early stages of the break-up of
1131 Gondwanaland. In: Storey, B.C., Alabaster, T., Pankhurst, R.J. (Eds.), Magmatism and the
1132 Causes of Continental Break-up. Geological Society, London, Special Publication, vol. 68,
1133 pp. 137-148.

1134 Cucchi, R., Busteros, A., Lema, H., 2001. Hoja Geológica 4169-II, Los Menucos, Provincia
1135 de Río Negro. IGRM-SEGEMAR. Boletin 265, Buenos Aires, 105 pp.

1136 Cúneo, R., Ramezani, J., Scasso, R., Pol, D., Escapa, I., Zavattieri, A.M., Bowring, S.A.,
1137 2013, High-precision U-Pb geochronology and a new chronostratigraphy for the Cañadón
1138 Asfalto Basin, Chubut, Central Patagonia: Implications for terrestrial faunal and floral
1139 evolution in Jurassic. Gondwana Research 24(3), 1267–1275.

1140 Delcourt, P.A., Delcourt, H.R.,1980. Pollen preservation and Quaternary environmental
1141 history in the southeastern United States. Palynology 4: 215–231.

1142 Dickinson, W.R., Gehrels, G.E., 2009. Use of U–Pb ages of detrital zircons to infer
1143 maximum depositional ages of strata: a test against a Colorado Plateau Mesozoic database.
1144 Earth and Planetary Science Letter 288(1–2), 115–125.

1145 Echaurren, A., Oliveros, V., Folguera, A., Ibarra, F., Creixell, C., Lucassen, F., 2017. Early
1146 Andean tectonomagmatic stages in north Patagonia: insights from field and geochemical
1147 data. Journal of the Geological Society 174 (3), 405-421.

1148 Encarnación, J., Fleming, T.H., Elliot, D.H., Eales, H.V., 1996. Synchronous emplacement
1149 of Ferrar and Karoo dolerites and the early break-up of Gondwana. Geology 24(6), 535-
1150 538.

1151 Falco, J.I., Bodnar, J., Hauser, N. 2017. Reinterpretación geológica de los depósitos
1152 clásticos del Graben del Co. Piche en la Comarca Nordpatagónica, Prov. de Rio Negro, In:
1153 Proc. XX Congreso Geológico Argentino (San Miguel de Tucumán), Actas Sección
1154 Técnica 1- Estratigrafía, 58–63.

1155 Franchi, M., Ardolino, A., and Remesal, M., 2001, Hoja Geológica 4166 III, Cona Niyeu,
1156 provincia de Río Negro: IGRM-SEGEMAR. Boletin 262, Buenos Aires, 83 pp.

1157 Franzese, J.R., Pankhurst, R. J., Rapela, C.W., Spalletti, L.A., Fanning, M., Muravchik, M.,
1158 2002. Nuevas evidencias geocronológicas del magmatismo gondwánico en el Noroeste del
1159 Macizo Norpatagonico. Actas Del XV Congreso Geológico Argentino, El Calafate, 1-5.

1160 Gerdes A., Zeh, A., 2009. Zircon formation versus zircon alteration - New insights from
1161 combined U–Pb and Lu–Hf in-situ LA-ICP-MS analyses, and consequences for the
1162 interpretation of Archean zircon from the Central Zone of the Limpopo Belt. Chemical
1163 Geology 261, 230-243.

1164 Gehrels, G.E., 2014. Detrital zircon U-Pb geochronology applied to tectonics. Annual
1165 Review of Earth and Planetary Sciences 42: 127-149.

1166 Giacosa, R.E., Lema, H., Busteros, A., Zubia, M., Cucchi, R., Tommaso, D.I., 2007.
1167 Estructura del Triásico de la región norte Macizo Nordpatagónico (40-41S, 67 30-69 45O)
1168 Río Negro. Revista de la Asociación Geológica Argentina 62(3), 355-365.

1169 Gnaedinger, S., Zavattieri, A., 2020. Coniferous woods from the Upper Triassic of
1170 southwestern Gondwana, Tronquimalal Group, Neuquén Basin, Mendoza Province,
1171 Argentina. Journal of Paleontology, 1-30.

1172 Haller, M., Linares, M., Ostera, H., Page, S., 1999. Petrology and geochronology of the
1173 Subcordilleran Plutonic Belt of Patagonia Argentina, in: Abstracts of the Second South
1174 American Symposium on Isotope Geology, Carlos Paz, Argentina, 210-214.

1175 Hauser, N., Cableri, N., Gallego, O., Monferran, M., Silva Nieto, D., Armella, C., Metteini,
1176 M., Aparicio González, P.A., Pimentel, M., Volkheimer, W., Reimold, W.U., 2017. U-Pb
1177 and Lu-Hf zircon geochronology of the Cañadón Asfalto Basin, Chubut, Argentina:
1178 Implications for the magmatic evolution in central Patagonia. Journal of South American
1179 Earth Sciences, http://doi.10.1016/j.jsames.2017.05.001.

1180 Heward, A., 1978. Alluvial fan and lacustrine sediments from the Stephanian A and B (La
1181 Magdalena, Ciñera – Matallana and Sabero) coalfields, northern Spain. Sedimentology
1182 25(4), 451-488.

1183 Jackson, S.E., Pearson, N.J., Griffina, W.L., Belousova, E.A., 2004. The application of
1184 laser ablation-inductively coupled plasma-mass spectrometry to in situ U–Pb zircon
1185 geochronology. Chemical Geology 211, 47-69.

1186 Labudía, C.H., Artabe, A., Morel, E., Bjerg, E., Gregori, D., 1992. El género Pleuromeia
1187 Corda (Lycophyta, Pleuromeiaceae) en sedimentitas triásicas de Coli Niyeu, Provincia de
1188 Rio Negro, Argentina. Ameghiniana 29(3), 195-199.

1189 Labudía, C.H., Bjerg, E.A., 1994. Geología del Sector Oriental de la Hoja Bajo Hondo
1190 (39e), Provincia de Río Negro. Revista de la Asociación Geológica Argentina 49, 284–296.

1191 Labudía, C.H., Bjerg, E.A., 2001. El Grupo Los Menucos: redefinición estratigráfica del
1192 Triásico superior del Macizo Nordpatagónico. Revista de la Asociación Geológica
1193 Argentina 56(3), 404-407.

1194 Leanza, H., Mazzini, A., Corfu, F., Llambías, E., Svensen, H., Planke, S., Galland, O.,
1195 2013. The Chachil Limestone (Pliensbachianeearliest Toarcian) Neuquén Basin, Argentina:
1196 UePb age calibration and its significance on the Early Jurassic evolution of southwestern
1197 Gondwana. Journal of South American Earth Science 42, 171-185.

1198 Lema, H., Busteros, A., Giacosa, R.E., Cucchi, R., 2008. Geología del Complejo volcánico
1199 Los Menucos en el área tipo - Río Negro. Revista de la Asociación Geológica Argentina
1200 63(1), 3-13.

1201 Lesta, P., Ferello, R., 1972. Región extrandina de Chubut y norte de Santa Cruz. In:
1202 Leanza, A.F., (Ed.), Geología Regional Argentina, Academia Nacional de Ciencias,
1203 Córdoba. pp. 601-687.

1204 Lizuaín, A., Silva Nieto, D., 2005. Observaciones Geológicas en la región de Río Chico,
1205 Gastre, río Chubut Medio, provincia del Chubut. In: 16 Congreso Geológico Argentino (La
1206 Plata), Actas, vol. 1, 133-139.

1207 Ludwig, K.R., 2012. User's Manual for Isoplot/Ex V. 3.0, a Geochronological Toolkit for
1208 Microsoft Excel. Berkley Geochronology Center, Berkeley, CA Special Publication No. 4,
1209 71 pp.

1210 Luppo, T., López de Luchi, M., Rapalini, A., Martínez Dopico, C., Fanning, C., 2017.
1211 Geochronologic evidence of a large magmatic province in northern Patagonia
1212 encompassing the Permian-Triassic boundary. Journal of South American Earth Sciences
1213 86, 335-346.

1214 Luppo, T., A., Martínez Dopico, Rapalini, A., López de Luchi, M., Miguez, M., Fanning,
1215 C. 2019. Paleomagnetism of Permo–Triassic volcanic units in northern Patagonia: are we
1216 tracking the final stages of collision of Patagonia? International Journal of Earth Science
1217 108: 621-647.

1218 Malvicini, L., Llambías, E., 1974. Geología y génesis del depósito de manganese Arroyo
1219 Verde, provincia del Chubut. In: V Congreso Geológico Argentino, Buenos Aires, Actas 2,
1220 pp. 185-202.

1221 Márquez, M., Massaferro, G.I., Fernández, M.I., Menegatti, N., Navarrete, C.R., 2012. El
1222 centro volcánico Sierra Grande: caracterización petrográfica y geoquímica del magmatismo
1223 extensional liásico, noroeste de la Patagonia. Revista de la Asociación Geológica Argentina
1224 68, 555-570.

1225 Martínez Dopico, C.I., López de Luchi, M.G., Rapalini, A.E., Fanning, C.M., Antonio,
1226 P.Y.J., 2019. Geochemistry and geochronology of the shallow-level La Esperanza
1227 magmatic system (Permian-Triassic), Northern Patagonia. Journal of South American Earth
1228 Science 96, 102347.

1229 Martínez Dopico, C.I., López de Luchi, M.G., Rapalini, A.E., Wemmer, K., Fanning, C.M.,
1230 Basei, M.A.S., 2017. Emplacement and temporal constraints of the Gondwanan intrusive
1231 complexes of northern Patagonia: La Esperanza plutono-volcanic case. Tectonophysics
1232 712-713, 249-269.

1233 Matteini, M., Dantas, E., Pimentel, M., Bühn, B., 2010. Combined U-Pb and Lu-Hf isotope
1234 analyses by laser ablation MC-ICP-MS: methodology and applications. Annals of the
1235 Brazilian Academy of Science 82(2), 479-491.

1236 Morel, M.L.A., Nebel, O., Nebel-Jacobsen, Y.L., Miller, J.S., Vroon, P.Z., 2008. Hafnium
1237 isotope characterization of the GJ-1 zircon reference material by solution and laser ablation
1238 MC-ICPMS. Chemical Geology 255, 231-235.
1239 Naipauer, M., Garcia Morabito, E., Manassero, M., Valencia, V., Ramos, V., 2018. A
1240 Provenance Analysis from the Lower Jurassic Units of the Neuquén Basin. Volcanic Arc or
1241 Intraplate Magmatic Input?. In: Folguera, A., Contreras-Reyes, E., Heredia, N., Encimas,
1242 A., Iannelli, S., Oliveros, V., Dávila, F., Collo, G., Giambiagi, L., Maksymowicz, A.,
1243 Iglesia Llanos, M.P., Turienzo, M., Naipauer, M., Orts, D., Litvak, V., Alvarez, O.,
1244 Arriagada, C. (Eds.) The Evolution of Chilean-Argentinian Andes. Springer Earth System
1245 Sciences, pp. 191-222.

1246 Nebel, O., Nebel-Jacobsen, Y., Mezger, K., Berndt, J., 2007. Initial Hf isotope
1247 compositions in magmatic zircon from early Proterozoic rocks from the Gawler Craton,
1248 Australia: A test for zircon model ages. Chemical Geology 241, 23-37.
1249 Nullo, F. E., Proserpio, C. 1975. La Formación Taquetrén en Cañadón del Zaino (Chubut) y
1250 sus relaciones estratigráficas en el ámbito de la Patagonia, de acuerdo a la flora. Revista de
1251 la Asociación Geológica Argentina 29 (3), 377–378.
1252 Nullo, F.E., 1978. Descripción Geológica de la Hoja 41d, Lipetrén, Provincia de Río
1253 Negro. Servicio Geológico Nacional, Buenos Aires, Boletín 158, 98 pp.
1254 Oboh-Ikuenobe, F., de Villiers, S., 2003. Dispersed organic matter in samples from the
1255 western continental shelf of Southern Africa: palynofacies assemblages and depositional
1256 environments of Late Cretaceous and younger sediments. Palaeogeography,
1257 Palaeoclimatology, Palaeoecology 201(1–2), 67-88.

1258 Pankhurst, R., Rapela, C., 1995. Production of Jurassic rhyolite by anatexis of the lower
1259 crust of Patagonia. Earth and Planetary Science Letters 134, 23-36.
1260 Pankhurst, R., Riley, T., Fanning, C., Kelley, S., 2000. Episodic silicic volcanism in
1261 Patagonia and the Antarctic Peninsula: chronology of magmatism associated with the
1262 break-up of Gondwana. Journal of Petrology 41, 605-625.
1263 Patchett, P.J., 1983. Importance of the Lu–Hf isotopic system in studies of planetary
1264 chronology and chemical evolution. Geochimica and Cosmochimica Acta 47, 81-89. DOI:
1265 10.1016/0016-7037(83)90092-3.
1266 Pavon Pivetta, C., Gregori, D., Benedini, L., Garrido, M., Strazzere, L., Geraldes, M.,
1267 Anderson Santos, C., Marcos, P., 2019. Contrasting tectonic settings in Northern Chon
1268 Aike Igneous Province of Patagonia: subduction and mantle plume-related volcanism in the
1269 Marifil Formation. International Geology Review 62, 1904-1930.
1270 Philippe, M., Bamford, M., McLoughlin, S., Alves, L.S.R., Falcon-Lang, H.J., Gnaedinger,
1271 S., Ottone, E.G., Pole, M., Rajanikanth, A., Shoemaker, R.E., Torres, T., and Zamuner, A.
1272 2004. Biogeographic analysis of Jurassic-Early Cretaceous wood assemblages from
1273 Gondwana. Review of Palaeobotany and Palynology 129: 141-173.

1274 Ramos, V.A., 1999. Las provincias geológicas del territorio argentino. In: Caminos, R.
1275 (Ed.). Geología Argentina. Instituto de Geología y Recursos Minerales, Anales 29(3) 41–
1276 96.

1277 Rapela, C., Pankhurst, R. 2020. The continental crust of northeastern Patagonia.
1278 Ameghiniana. doi: 10.5710/AMGH.17.01.2020.3270.

1279 Rapela, C. W., Pankhurst, R. J., Fanning, C. M., Hervé, F. 2005. Pacific subduction coeval
1280 with the Karoo mantle plume: the Early Jurassic Subcordilleran Belt of northwestern

Patagonia. In: Vaughan, A.P.M., Leat, P. T., Pankhurst, R.J. (Eds.), Terrane Accretion Processes at the Pacific Margin of Gondwana. The Geological Society, Special Publication 246, pp. 217–239.

Riley, T.R., Knight, K.B., 2001. Age of pre-break-up Gondwana magmatism: a review. Antarctic Science 13, 99-110.

Rolando, A., Hartmann, L., Santos, J., Fernandez, R., Etcheverry, R., Schalamuk, I., Mcnaughton, N., 2002. SHRIMP zircon U-Pb evidence for extended Mesozoic magmatism in the Patagonian batholith and assimilation of Archaean crustal components. Journal of South American Earth Science 15, 267–283.

Rossel, P., Echaurren, A., Ducea, M., Maldonado, P., Llanos, K., 2020. Jurassic segmentation of the early Andean magmatic Province in southern central Chile (35–39°S): Petrological constrains and tectonic drivers. Lithos 364-365, 1-20.

Rossignol C., Hallot, E., Bourquin, S., Poujol, M., Jolivet, M., Pellenard, P., Ducassou, C., Nalpas, T., Heilbronn, G., Yu, J., Dabard, M., 2019. Using volcaniclastic rocks to constrain sedimentation ages: To what extent are volcanism and sedimentation synchronous? extent are volcanism and sedimentation synchronous?. Sedimentary Geology 381, 46-64.

Sato, A.M., Basei, M., Tickyj, H., Llambías, E., Varela, R., 2004. Granodiorita El Sótano: plutón jurásico deformado aflorante en el basamento de Las Grutas, Macizo Norpatagónico Atlántico. Revista de la Asociación Geológica Argentina 59(4), 591-600.

Scherer, E., Münker, C., Mezger, K., 2006. Calibration of the lutetium-hafnium clock. Science 293, 683-687.

Sharman, G., Malkowski, M. 2020. Needles in a haystack: Detrital zircon U-Pb ages and the máximum depositional age of modern global sediment. Earth-Science Reviews 203, 103109.

1305 Silva Nieto, D., Cabaleri, N., Salani, F., Coluccia, A., 2002. Cañadón Asfalto, una cuenca
1306 de tipo “Pull apart” en el área de Cerro Cóndor. Provincia del Chubut. 15 Congreso
1307 Geológico Argentino, Calafate, 238-243.
1308 Siivola, J., Schmid, R., 2007. List of Mineral Abbreviation. In: Fettes, D., Desmonds, J. (Eds.).
1309 Metamorphic Rocks. A Classification and Glossary of Terms. Cambridge University Press,
1310 Cambridge, pp. 93-110.
1311 Stipanicic, P.N., Rodrigo, F., Baulies, O. L., Martínez, C.G., 1968. Las formaciones
1312 presenonianas en el denominado Macizo Nordpatagónico y regiones adyacentes. Revista de
1313 la Asociación Geológica Argentina 23, 37–53.
1314 Storey, B.C., Vaughan, A.P.M., Riley, T.R., 2013. The links between large igneous
1315 provinces, continental break-up and environmental change: evidence reviewed from
1316 Antarctica. Earth and Environmental Science Transactions of the Royal Society of
1317 Edinburgh 104, 1-14.
1318 Strazzere, L., Gregori, D., Benedini, L., Marcos, P., Barros, M., Geraldes, M., Pavon
1319 Pivetta, C., 2018. The Puesto Piris Formation: Evidence of basin-development in the North
1320 Patagonian Massif during crustal extension associated with Gondwana breakup. Geoscience
1321 Frontiers 10(1), 299-314.
1322 Strazzere, L., Gregori, D., Benedini, L., Marcos, P., Barros, M., 2017. Edad y petrografía
1323 del Complejo Volcánico Marifil en la Sierra de Paileman, Comarca Nordpatagónica, Rio
1324 Negro, Argentina, in: Proc. XX Congreso Geológico Argentino, Actas, pp. 1026-1031.
1325 Taylor, S.R., McLennan, S.M., 1985. The Continental Crust: its Composition and
1326 Evolution. Blackwell, Oxford, U.K., 312pp.
1327 Traverse, A., ed., 1994. Sedimentation of Organic Particles. Cambridge University Press,
1328 533 pp.

1329 Tyson, R., 1995. Sedimentary Organic Matter. Chapman and Hall, London, 615 pp.

1330 Wedepohl, K.H., 1995. The compositions of the continental crust. Geochimica et
1331 Cosmochimica Acta 59, 1217-1232.

1332 Wiedenbeck, M., Allé, P., Corfu, F., Griffin, W., Meier, M., Oberli, F., Quadt, A.V.,
1333 Roddick, J., Spiegel, W., 1995. Three natural zircon standards for U-Th-Pb, Lu-Hf, trace
1334 elements and REE analyses. Geostandards Newsletter, 19: 1-23.

1335 Wiedenbeck, M.P., Hanchar, J.M., Peck, W.H., Sylvester, P., Valley, J., Whitehouse, M.,
1336 Kronz, A., Morishita, Y., Nasdala, L., Fiebig, J., Franchi, I., Girard, J-P., Greenwood, R.C.,
1337 Hinton, R., Kita, N., Mason, P.R.D., Norman, M., Ogasawara, M., Piccoli, P.M., Rhede, D.,
1338 Satoh, H., Schulz-Dobrick, B., Skår, O., Spicuzza, M.J., Terada, K., Tindle, A., Togashi, S.,
1339 Vennemann, T., Xie, Q., Zheng, Y-F., 2004. Further characterisation of the 91500 zircon
1340 crystal. Geostandards and Geoanalytical Research 28, 9–39.

1341 Zaffarana, C., Lagorio, S., Gallastegui, G., Wörner, G., Orts, D., Gregori, D., Poma, S.,
1342 Busteros, A., Giacosa, R., Nieto, D.S., Ruíz González, V., Boltshauser, B., Puigdomenech,
1343 C., Haller, M., 2020. Petrogenetic study of the Lonco Trapial volcanism and its comparison
1344 with the early-middle Jurassic magmatic units from northern Patagonia. Journal of South
1345 American Earth Sciences 101, 102624.

1346 Zappettini, E., Lagorio, S., Dalponte, M., Santos, J., Belousova, E., 2018. Evidencias de
1347 magmatismo precuyano (Pliensbachiano - Toarciano) en el norte de la Cordillera del
1348 Viento, provincia del Neuquén: caracterización geoquímica, isotópica e implicancias
1349 tectónicas. Revista de la Asociación Geológica Argentina 75(4), 533-558.

- A combined U-Pb/Hf isotope study related to the evolution of the Cerro Piche graben, northern Patagonia, Argentina is reported.
- A new U-Pb in zircon age of 183 Ma indicate that the Cerro Piche Graben is Jurassic in age, contrasting with the previous Early-Middle Triassic age.
- Stratigraphic, sedimentological and paleontological analyses are also integred to the understanding of this basin.
- Four magmatic cycles (C0-C3) with different Hf isotopic characteristics are recognized for northern Patagonia

Declaration of interests

☒ The authors declare that they have no known competing financial interests or personal relationships that could have appeared to influence the work reported in this paper.

☐The authors declare the following financial interests/personal relationships which may be considered as potential competing interests: